CH_2=C*H*—CH=CH_2), 4.600 (m, 1, CH_2=CH—C*H*=CH_2), 1.380 (d, 9, $^2J_{HP}$ = 7.3 Hz, PMe_3), 0.957 (d, 9, $^2J_{HP}$ = 6.7 Hz, PMe_3'), 2.23, 1.44, 1.15, 1.00, 0.842, -0.161, -0.807, -0.919 (m, 1, olefinic resonances). The 4.826- and 4.600-ppm resonances coalesce at 75 ± 10 °C [$\Delta\nu$ = 62 ± 5 Hz, $\Delta G^{\ddagger}$ = 17 ± 1 kcal mol^{-1}]. ^{13}C NMR (toluene-d_8, 67.89 MHz, -30 °C): 94.87 (d, $^1J_{CH}$ = 160 Hz, CH_2=*C*H—CH=CH_2), 92.57 (d, $^1J_{CH}$ = 163 Hz, CH_2=CH—*C*H=CH_2), 51.79 (tt, $^2J_{CP}$ = 5.6 Hz, $^1J_{CH}$ = 147 Hz, *C*H_2=CH_2), 43.40 (ddd, $^2J_{CP}$ = 5.7 Hz, $^1J_{CH}$ = 155 and 148 Hz, CH_2=*C*H_2), 34.75 (ddd, $^2J_{CP}$ = 7.8 Hz, $^1J_{CH}$ = 141 and 149 Hz, *C*H_2=CH—CH=CH_2), 30.19 (tt, $^2J_{CP}$ = 8.2 Hz, $^1J_{CH}$ ≈ 150 Hz, CH_2=CH—*C*H=CH_2), 14.92 (qd, $^1J_{CP}$ = 21.6 Hz, $^1J_{CH}$ = 130 Hz, PMe_3), 13.54 (qd, $^1J_{CP}$ = 23.3 Hz, $^1J_{CH}$ = 130 Hz, PMe_3'). ^{13}C NMR (15.0 Hz, 60 °C): ethylene carbon atom resonances coalesce [T_c = 60 ± 10 °C, $\Delta\nu$ = 129 ± 5 Hz, $\Delta G^{\ddagger}$ = 16 ± 1 kcal mol^{-1}]. ^{13}C NMR (15.0 MHz, 100 °C): 93.95 (s, CH_2=*C*H—*C*H=CH_2), 47.8 (br s, *C*H_2=*C*H_2), 33.1 (s, *C*H_2=CH—CH=*C*H_2), 14.9 ppm (d, $^1J_{CP}$ ≈ 12 Hz, PMe_3). ^{31}P NMR ($CDCl_3$, 109.3 MHz, -30 °C): δ 2.0 (s) and -8.3 (s) (major isomer), 2.5 (s) and -7.8 (s) (minor isomer). The ratio of the major to minor isomer was 2:1 at -30 °C for this sample in this solvent.

(14) Ta(1,3-butadiene)(C_2H_4)(Et)(PMe_3)$_2$. Ta(C_4H_6)(C_2H_4)(Cl)(PMe_3)$_2$ (1.25 g, 2.77 mmol) was dissolved in ether (25 mL), and the solution was cooled to -78 °C. A 4.7-mL sample of a 1.18 M LiC_2H_5 (excess) in benzene solution was added slowly by syringe. The reaction mixture was warmed to 25 °C, stirred for 30 min, and filtered. The solvent was removed in vacuo, and the residue was recrystallized from minimal pentane; yield 0.6 g (49%).

Anal. Calcd for $TaC_{14}H_{33}P_2$: C, 37.84; H, 7.48. Found: C, 37.23; H, 7.32. ^{1}H NMR (toluene-d_8, 270 MHz, -40 °C): δ 4.92 (m, CH_2=C*H*—CH=CH_2), 3.46 (m, CH_2=CH—C*H*=CH_2), 1.30 (d, $^2J_{HP}$ ≈ 6 Hz, PMe_3), 0.87 (d, $^2J_{HP}$ ≈ 6 Hz, PMe_3'), 1.55, 1.16, 0.76, -0.16, and -0.37 (m, olefinic and CH_2 resonances), -0.05 (t, $^3J_{HH}$ = 7.7 Hz, CH_2CH_3). ^{13}C NMR (toluene-d_8, 67.89 MHz, -40 °C): major isomer, 102.3 (d, $^1J_{CH}$ = 157 Hz, CH_2=*C*H—CH=CH_2), 89.0 (d, $^1J_{CH}$ = 163 Hz, CH_2=CH—*C*H=CH_2), 48.6 ppm (tt, $^2J_{CP}$ = 5.7 Hz, $^1J_{CH}$ = 146 Hz, *C*H_2=CH_2), 42.1 (td, $^2J_{CP}$ = 4.8 Hz, $^1J_{CH}$ = 149 Hz, CH_2=*C*H_2), 33.9 (td, $^2J_{CP}$ = 5.8 Hz, $^1J_{CH}$ = 150 Hz, *C*H_2—CH—CH=CH_2), 33.6 (t, $^1J_{CH}$ = 116 Hz, *C*H_2CH_3), 25.1 (td, $^2J_{CP}$ = 9.0 Hz, $^1J_{CH}$ = 149 Hz, CH_2=CH—CH=*C*H_2), 15.0 (qd, $^1J_{CP}$ = 17.7 Hz, $^1J_{CH}$ ≈ 130 Hz, PMe_3), 13.5 (qd, $^1J_{CP}$ = 19.4 Hz, $^1J_{CH}$ ≈ 130 Hz, PMe_3'), 5.8 ppm (q, $^1J_{CH}$ = 123 Hz, CH_2CH_3); minor isomer, 94.4 (CH_2=*C*H—CH=CH_2), 92.3 (CH_2=CH—*C*H=CH_2), 51.7 (*C*H_2=CH_2), 43.2 (CH_2=*C*H_2), 1.55 ppm (CH_2CH_3). (Other signals could not be found in this sample.) ^{31}P NMR (toluene-d_8, 109.3 MHz, -47 °C): δ -6.4 (s) and -11.4 (s) (major isomer), -6.0 (s) and -11.9 (s) (minor isomer). The ratio of the major to minor isomer was 3:1 at -47 °C and 1:1 at 30 °C.

Acknowledgment. We thank the National Science Foundation for support (Grant CHE 79-05307), and the donors of the Petroleum Research Fund, administered by the American Chemical Society, for partial support in the form of a fellowship to G.A.R. We also want to thank D. Traficante for helpful discussions, and Andrew Schkuta of Professor K. Biemann's group for determining the exact mass of Ta($CHCMe_3$)$_2$(Cl)(PMe_3)$_2$ at the NIH Mass Spectroscopy Facility (Grant No. RR00317).

Thioether Ligation in Iron-Porphyrin Complexes: Models for Cytochrome *c*

Toshio Mashiko,[1] Christopher A. Reed,*[1] Kenneth J. Haller,[2] Margaret E. Kastner,[2] and W. Robert Scheidt*[2]

Contribution from the Departments of Chemistry, University of Notre Dame, Notre Dame, Indiana 46556, and University of Southern California, Los Angeles, California 90007.
Received December 22, 1980. Revised Manuscript Received May 20, 1981

Abstract: Iron-*meso*-tetraphenylporphyrin complexes having thioether ligation have been synthesized and investigated as models for cytochrome *c*. Using a 5-(*N*-imidazoyl)valeramido-derivatized "tail porphyrin" of iron(II) and tetrahydrothiophene, it was possible to isolate a mixed-ligand complex having thioether imidazole coordination, [*meso*-mono[*o*-(5-(*N*-imidazolyl)-valeramido)phenyl]triphenylporphinato](tetrahydrothiophene)iron(II) (**1**). The crystal structure of **1** was determined. An analogous iron(III) model for ferricytochrome *c* was characterized by EPR in solution (g = 2.90, 2.37, 1.48). A structural comparison between the iron(II)/iron(III) redox pair of complexes bis(tetrahydrothiophene)(*meso*-tetraphenylporphinato)iron(II) (**5**) and bis(pentamethylene sulfide)(*meso*-tetraphenylporphinato)iron(III) perchlorate (**7**) was made by X-ray analysis and reveals Fe-S bond lengths which are notably insensitive to oxidation state change. The structural analysis for bis(tetrahydrothiophene)(*meso*-tetraphenylporphinato)iron(III) perchlorate (**6**) is also briefly reported. All complexes have low-spin ground states. The main implications for cytochrome *c* are as follows: (i) Fe-S bond lengths in methionine-ligated hemoproteins are expected to be about 2.33 Å and rather insensitive to oxidation state change, (ii) coordinate bond length changes are unlikely to contribute to Franck-Condon barriers of electron transfer, and (iii) the intrinsic stability of the Fe(III)-S(thioether) bond is sufficiently high that a protein conformation-enforced methionine-iron contact need not be invoked. Crystal data: **1**, a = 13.170 (4) Å, b = 15.037 (11) Å, c = 25.422 (8) Å, β = 90.29 (2)°, monoclinic, space group $P2_1/c$, Z = 4; **5**, a = 13.225 (3) Å, b = 17.967 (5) Å, c = 10.283 (2) Å, α = 91.07 (2)°, β = 99.22 (2)°, γ = 76.59 (2)°, triclinic, space group $P\bar{1}$, Z = 2; **7**, a = 17.830 (3) Å, b = 18.781 (3) Å, c = 18.187 (3) Å, orthorhombic, space group $P2_12_12_1$, Z = 4; **6**, a = 13.007 (7) Å, b = 19.188 (9) Å, c = 11.256 (5) Å, α = 93.99 (3)°, β = 107.17 (4)°, γ = 95.01 (4)°, triclinic, space group $P1$, Z = 2.

The cytochromes are a widely distributed class of electron carriers having heme prosthetic groups. The reversible iron(II)/iron(III) valency change enables the cytochromes to function in numerous biological redox processes, and the prototypical cytochromes *c* have commanded much attention. Following the elucidation of the first crystal structure of a cytochrome *c* in 1971, the problem of understanding its mechanism of electron transfer became the central focus of cytochrome research.[3,4] The two most contentious issues, the pathway of electron transfer and the factors affecting the rate, remain incompletely resolved although considerable progress has been made.[5,6] Intimately related to these

(1) University of Southern California.
(2) University of Notre Dame.

(3) Dickerson, R. E.; Timkovich, R. "The Enzymes"; Boyer, P., Ed.; Academic Press: New York, 1975, Vol XI; pp 397-547.
(4) Salemme, F. R. *Annu. Rev. Biochem.* **1977**, *46*, 327-386.

0002-7863/81/1503-5758$01.25/0

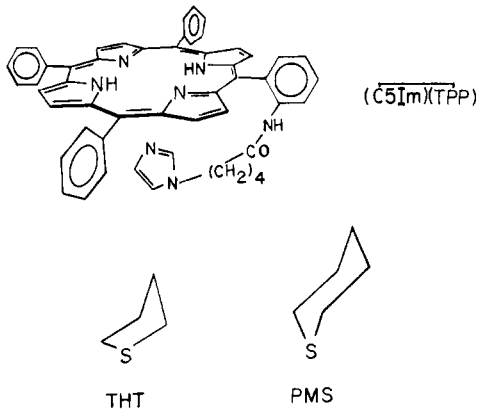

Figure 1. Schematic drawings of the structures of tetrahydrothiophene (THT), pentamethylene sulfide (PMS), and (C5Im)(TPP).

kinetic aspects are the thermodynamic aspects of redox potential, ligand binding affinities, and the structural changes upon valency change. In this paper,[7] we explore how the model compound approach[8] can contribute to an understanding of these aspects, particularly with respect to the structural features of thioether ligation.

Methionine coordination to iron, together with histidine, is present in all the cytochromes *c* and has recently been established for a *b*-type cytochrome.[9] Excepting that it has been known for some time that thioether ligation is weaker than imidazole, little is known about the intrinsic properties of thioether ligation to iron porphyrins. A protein conformation-enforced contact between the methionine ligand and iron has been invoked for cytochrome *c* especially for the low-spin ferric form.[10] Early model studies,[11-17] though frequently admirable achievements of synthetic chemistry, were restricted to spectral studies in solution. A central question is what is the biochemical rationale behind the persistent occurrence of methionine as a ligand in cytochromes *c*. The effect of methionine ligation in raising the redox potential, the possible contribution to Franck–Condon barriers to electron transfer, expectations for Fe–S bond lengths in hemoproteins, and an appreciation of protein constraints on the heme coordination group are all questions which can be addressed by studying synthetic analogues. It is only coincident with this publication that an accurate assessment of redox conformation changes in cytochrome *c* has become available from refined protein X-ray crystal structure analyses.[18]

Experimental Section

Synthesis. Air-sensitive iron(II) species and water-sensitive iron(III) species were handled under an inert atmosphere in a glovebox or in Schlenk tubes. In general, methods and reagents were as previously reported.[19] Tetrahydrothiophene (THT)[20] and pentamethylene sulfide (PMS) were carefully distilled prior to use to remove sulfoxides. The structures of THT, PMS, and (C5Im)(TPP) are given in Figure 1.

Fe(C5Im)(TPP)·C_6H_6 (1). *meso*-Mono[*o*-(5-(*N*-imidazolyl)valeramido)phenyl]triphenylporphyrin[21] (234 mg), $FeBr_2$ (216 mg) and 1,8-bis(dimethylamino)naphthalene (Aldrich "proton sponge") (62 mg) were dissolved in a mixture of benzene (7 mL) and tetrahydrofuran (7 mL), and the mixture was heated under reflux for 30 min. After being cooled, the mixture was passed down a short silica gel column, eluting first with benzene and then with benzene–methanol (10:1). The red fraction was collected and evaporated to dryness under vacuum. The purple product was redissolved in benzene (30 mL) and tetrahydrothiophene (35 mg) was added. After the solution was mixed, heptane (50 mL) was carefully layered above the benzene and the Schlenk tube set aside. After several days, purple crystals were deposited. These were collected by filtration and washed with heptane (200 mg, 67%): IR (KBr) ν(NH) 3400, ν(CO) 1690 cm^{-1}; the material was essentially diamagnetic ($\mu_{eff}^{26°C} = 0.7\ \mu_B$); GLC analysis for THT, calcd 8.8, found 8.4, for benzene, calcd 7.8, found 6.5; λ_{max} (toluene) 433, 534, 560, 610 nm. Anal. Calcd for $C_{62}H_{53}ON_7SFe$: C, 74.46; H, 5.34; N, 9.89. Found: C, 74.42; H, 5.47; N, 9.57. Several other related complexes with C4 or C6 tails and with other thioethers (e.g., PMS) were synthesized by similar methods, but since nicely crystalline materials were not obtained, these materials were not fully investigated.

[Fe(C5Im)(TPP)]ClO_4·THF (4). The benzene solution of Fe(C5Im)(TPP) from above (after chromatography) was exposed to air to form a presumed μ-oxo derivative which was isolated as a purple powder by evaporation under reduced pressure. This material (1.0 g) was dissolved in chloroform (50 mL) and the mixture acidified by adding chloroform (40 mL) which had been freshly saturated with dry HCl. After the solution was evaporated to dryness, the resulting oil was taken up into hot toluene, filtered, and again evaporated to dryness. Upon dissolution in warm THF (50 mL), treatment with 1,8-bis(dimethylamino)naphthalene (250 mg) gave a brown-red solution of presumed Fe(C5Im)(TPP)Cl which yielded a purple powder with heptane (30 mL) (0.8 g, 77%) ($\mu_{eff}^{25°C} = 5.4\ \mu_B$). Treatment of this material (174 mg) with AgClO (41 mg) in hot THF (5 mL) gave a white precipitate which was filtered off. Addition of heptane to the fitrate gave a purple powder which was reprecipitated from tetrahydrofuran–heptane (110 mg, 55%): $\mu_{eff}^{25°C} = 4.5\ \mu_B$; EPR ($CH_2Cl_2$–$CHCl_3$) g = 2.86, 2.28, 1.58 and g = 5.90, 1.99; EPR of the PMS adduct (CH_2Cl_2–$CHCl_3$–excess PMS) g = 2.90, 2.37, 1.48. Anal. Calcd for $C_{56}H_{47}O_6N_7ClFe$: C, 66.85; H, 4.71; N, 9.76. Found: C, 66.22; H, 4.68; N, 9.40.

$Fe(THT)_2(TPP)$·THT (5). A THF solution (35 mL) of Fe(TPP) (100 mg) was treated with excess tetrahydrothiophene (2 mL), and upon gradual addition of heptane purple crystals were deposited (110 mg, 90%): diamagnetic, $\chi_M^{uncorr} = -5.5 \times 10^6$ cgs units. Anal. Calcd for $C_{56}H_{52}N_4S_3Fe$: C, 72.08; H, 5.62; N, 6.01. Found: C, 72.01; H, 5.70; N, 6.11.

[$Fe(THT)_2(TPP)$]ClO_4·1.5$CHCl_3$ (6). A mixture of $Fe(OClO_3)$(TPP)·0.5C_7H_8[22] (100 mg) and tetrahydrothiophene (2 mL) in chloroform (10 mL) was heated gently for 5 min. To the filtered solution was carefully added a layer of heptane, and the Schlenk tube was set aside in a freezer (−18 °C) for several days. The purple crystals were filtered off and washed with cold heptane (140 mg, 86%): IR (KBr) $\nu(ClO_4)$ 1090, 615 cm^{-1}; $\mu_{eff}^{26°C} = 2.06\ \mu_B$; GLC analysis for THT, calcd 15.7, found 13.1, for $CHCl_3$, calcd 15.9, found 17.1; λ_{max} (CH_2Cl_2–excess THT) 417, 506, 546, 580 nm; EPR (CH_2Cl_2–$CHCl_3$–excess THT) g = 2.91, 2.37. Anal. Calcd for $C_{53.5}H_{45.5}O_4N_4S_2Cl_{3.5}Fe$: C, 57.20; H, 4.08; N, 4.99. Found: C, 57.44; H, 4.30; N, 5.15.

[$Fe(PMS)_2(TPP)$]ClO_4·3$CHCl_3$ (7). This was prepared as above: $\mu_{eff}^{26°C} = 2.10\ \mu_B$; λ_{max} (CH_2Cl_2–excess PMS) 420, 507, 545, 580 nm; EPR (CH_2Cl_2–$CHCl_3$–excess PMS) g = 2.91, 2.37. Anal. Calcd for

(5) Sutin, N. "Bioinorganic Chemistry II", *Adv. Chem. Ser.* **1977**, *No. 162*, 156-172.
(6) Mauk, A. G.; Coyle, C. L.; Bordignon, E.; Gray, H. B. *J. Am. Chem. Soc.* **1979**, *101*, 5054-5056.
(7) For a preliminary account see: Mashiko, T.; Marchon, J.-C.; Musser, D. T.; Reed, C. A.; Kastner, M. E.; Scheidt, W. R. *J. Am. Chem. Soc.* **1979**, *101*, 3653-3655.
(8) Ibers, J. A.; Holm, R. H. *Science (Washington, D.C.)* **1980**, *209*, 223-235.
(9) Xavier, A. U.; Czerwinski, E. W.; Bethge, P. H.; Matthews, F. S. *Nature (London)* **1978**, *275*, 245-247. Mathews, F. S.; Bethge, P. H.; Czerwinski, E. W. *J. Biol. Chem.* **1979**, *254*, 1699-1706.
(10) Lemberg, R.; Barrett, J. "Cytochromes"; Academic Press: London and New York, 1973; pp 160-161.
(11) Harbury, H. A.; Cronin, J. R.; Fanger, M. W.; Hettiger, T. P.; Murphy, A. J.; Meyer, Y. P.; Vinogradov, S. N. *Proc. Natl. Acad. Sci. U.S.A.* **1965**, *54*, 1658-1664.
(12) Schechter, E.; Saludjian, P. *Biopolymers* **1967**, *5*, 788-790.
(13) Warme, P. K.; Hager, L. P. *Biochemistry* **1970**, *9*, 1599-1614.
(14) Schejter, A.; Aviram, I.; Maralit, R.; Goldkorn, T. *Ann. N. Y. Acad. Sci.* **1975**, *244*, 51-59.
(15) Castro, C. E. *Bioinorg. Chem.* **1974**, *4*, 45-65.
(16) Momenteau, M.; Rougee, M.; Loock, B. *Eur. J. Biochem.* **1976**, *71*, 63-76.
(17) Buckingham, D. A.; Rauchfuss, T. B. *J. Chem. Soc., Chem. Commun.* **1978**, 705-707.
(18) Takano, T.; Dickerson, R. E. In "Interaction Between Iron and Proteins in Oxygen and Electron Transport", Ho, C., et al., Eds.; Elsevier/North Holland: New York; in press; Takano, T.; Dickerson, R. E. *Proc. Natl. Acad. Sci. U.S.A.* **1980**, *77*, 6371-6375.
(19) Landrum, J. T.; Hatano, K.; Scheidt, W. R.; Reed, C. A. *J. Am. Chem. Soc.* **1980**, *102*, 6729-6735.
(20) Abbreviations used in this paper: THT, tetrahydrothiophene; PMS, pentamethylene sulfide; TPP, dianion of *meso*-tetraphenylporphyrin.
(21) Collman, J. P.; Brauman, J. I.; Doxsee, K. M.; Halbert, T. R.; Bunnenberg, E.; Linder, R. E.; LaMar, G. N.; Del Gaudio, J.; Lang, G.; Spartalian, K. *J. Am. Chem. Soc.* **1980**, *102*, 4182-4192.
(22) Reed, C. A.; Mashiko, T.; Bentley, S. P.; Kastner, M. E.; Scheidt, W. R.; Spartalian, K.; Lang, G. *J. Am. Chem. Soc.* **1979**, *101*, 2948-2958.

$C_{57}H_{51}O_4N_4S_2Cl_{10}Fe$: C, 51.46; H, 3.86; N, 4.21. Found: C, 52.23; H, 4.11; N, 4.20.

X-ray Structure Determinations. All crystals were subjected to preliminary examination on a Syntex $P\bar{1}$ diffractometer. Least-squares refinement of the setting angles for several reflections, collected at $\pm 2\theta$, gave the cell constants reported in Table I. For the low-temperature measurements, a Syntex LT-1 attachment to the diffractometer was employed. All measurements utilized graphite-monochromated Mo Kα radiation ($\lambda = 0.71073$ Å). Details of the intensity collection parameters are summarized in Table I. Data were reduced as described previously.[23] All structures were solved by using heavy-atom methods[24] utilizing standard values for atomic scattering factors.[25] All data sets were corrected for absorption effects.

Fe(THT)$_2$(TPP)·THT (5). The unit cell of this compound contains two molecules. A Patterson function was consistent only with unique iron atom positions of 0, 0, 0 and 0, $^1/_2$, $^1/_2$. Thus the iron atoms are located at centers of symmetry in space group $P\bar{1}$; the crystallographically unique atoms are those for two half molecules of Fe(THT)$_2$(TPP), each with a required center and a THT solvent molecule in a general position. All subsequent developments of structure solution and refinement were consistent with the choice of $P\bar{1}$ as the space group. After several cycles of block-diagonal least-squares refinement, a difference Fourier synthesis showed the positions of all hydrogen atoms of the porphinato ligand and most of the THT ligand hydrogen atoms. These hydrogen atom positions were idealized (C–H = 0.95 Å for porphinato hydrogen atoms and 1.0 Å for THT, B(H) = B(C) + 1.0 Å^2) and included in subsequent refinement cycles as fixed contributors. The refinement was carried to convergence by using anisotropic temperature factors for all heavy atoms. A final difference Fourier synthesis was judged to show no significant features with the largest peak of 0.64 e/Å^3. A listing of the final observed and calculated structure amplitudes is available as supplementary material. Atomic coordinates and the associated anisotropic temperature factors in the asymmetric unit of structure are listed in Tables II and III and are available as supplementary material.

[Fe(THT)$_2$(TPP)]ClO$_3$·1.5CHCl$_3$ (6). The Patterson map suggested iron atom positions of 0, 0, 0 and 0, $^1/_2$, $^1/_2$, i.e., the [Fe(THT)$_2$(TPP)]$^+$ moieties have required inversion centers. Refinement of a data set collected at room temperature was unsatisfactory. The temperature factors of the ion centered at 0, $^1/_2$, $^1/_2$ were considerably larger than those of the ion at 0, 0, 0. The ligand on this ion also appeared disordered. In an attempt to solve these problems, a new data set was collected at low temperatures. As was also noted at room temperature, a significant amount of crystal decomposition occurred during exposure to the X-ray beam and a linear correction was applied. Refinement of this new data set was also judged to be unsatisfactory. In addition to the high discrepancy indices, the thermal parameters of the ion at 0, $^1/_2$, $^1/_2$ were approximately 1.6 times those of the ion at 0, 0, 0. We were unable to account for this systematic variation. All final parameters (coordinates, temperature factors, bond distances and angles) are reported in Tables IV–VII of the supplementary material.

[Fe(PMS)$_2$(TPP)]ClO$_4$·3CHCl$_3$ (7). The structure consists of one full molecule in the asymmetric unit. The hydrogen atoms were found as before and included as fixed contributors. One chloroform molecule of solvation was found to be disordered and had two orientations. The positions of the six chlorine atoms were accordingly assigned occupancy factors of 0.5 and refined by using isotropic temperature factors. The refinement was carried to convergence by using anisotropic temperature factors for all other heavy atoms. The final R_1 was 0.077 and R_2 was 0.086. Further refinement, using coordinates of the mirror image of the enantiomorph previously assumed, led to R_1 = 0.080 and R_2 = 0.090. The first choice is clearly the correct one, and its coordinates are reported herein. A final difference Fourier synthesis had no peaks larger than 0.7 e/Å^3, and the highest peaks were all associated with the anion or the solvent molecules. A listing of the final observed and calculated structure amplitudes is available as supplementary material. The atomic coordinates and associated anisotropic thermal parameters of [Fe(PMS)$_2$(TPP)]ClO$_4$·3CHCl$_3$ are listed in Tables VIII and IX and are available as supplementary material.

Fe(C5Im)(TPP)(THT)·C$_6$H$_6$ (1). This structure was originally determined from a room temperature data set.[7] Significant crystal decomposition occurred during data collection, and only a limited data set was available. This structure did however provide confirmation of the synthetic chemistry. In order to significantly improve the structure quality, we remeasured diffraction data, utilizing a freshly prepared crystal, at −175 °C. The refinement of this data set did yield a much more precise structure and, in addition, revealed three difficulties of the crystalline sample which were probably also present in the crystal used for the room-temperature data set. These are the presence of ~3.4 (4)% high-spin ferric impurity, a loss of ~12% of the axial THT ligand, and the partial presence of an additional substituent (at C_{23}) of the phenyl ring bearing the tail substituent. The presence of a small amount of a ferric contaminant in tail porphyrins has been observed previously.[21] It is not clear whether the loss of the THT occurred during or prior to data collection. The presence of an additional substituent (assumed to be a CH_3 group at ~35% for refinement) was surprising as this was not discernible from the NMR spectrum of the ligand. A halide substituent

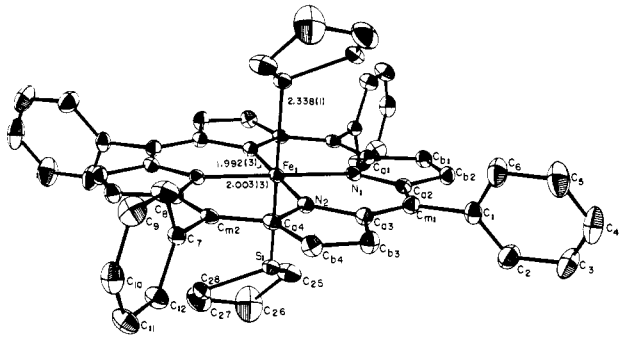

Figure 2. An ORTEP drawing of molecule 1 of Fe(THT)$_2$(TPP). The atom labels assigned to the crystallographically unique atoms are shown. Also displayed are the unique bond distances around the iron atom. 50% probability ellipsoids are given.

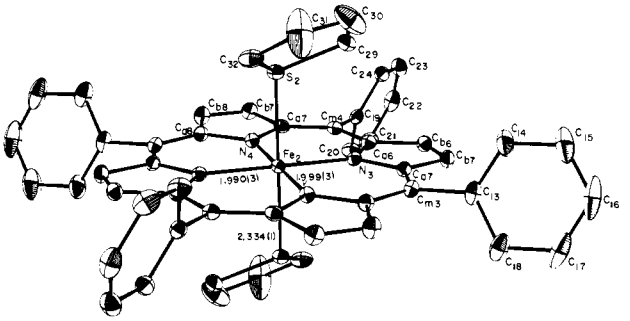

Figure 3. An ORTEP drawing of molecule 2 of Fe(THT)$_2$(TPP). The same information as in Figure 2 is given.

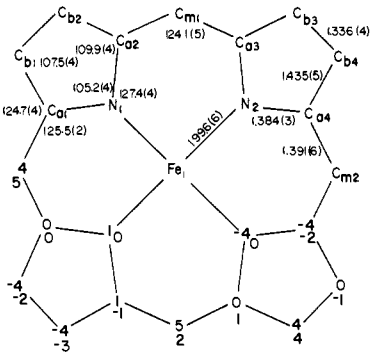

Figure 4. A formal diagram of a porphinato core displaying for Fe(THT)$_2$(TPP) the averaged values of the unique chemical types of bond distances and bond angles. The numbers in parentheses are the estimated standard deviations calculated on the assumption that all values are drawn from the same population. On the lower half of the diagram the perpendicular displacements, in units of 0.01 Å, of each atom from the mean plane of the 24-atom core are shown. The upper value of each pair of values is that for molecule 1, the lower is that for molecule 2. The displacements of the centrosymmetrically related atoms are of the same magnitude and opposite sign.

(23) Scheidt, W. R. *J. Am. Chem. Soc.* **1974**, *96*, 84–89.

(24) Programs used in this study included local modifications of Jacobson's ALFF, Park's REFINE, Busing and Levy's ORFFE and ORFLS, and Johnson's ORTEP2.

(25) Atomic form factors were from Cromer, D. T.; Mann, J. B. *Acta Crystallogr., Sec. A* **1968**, *A24*, 321–323, with real and imaginary corrections for anomalous dispersion in the form factor of the iron chlorine and sulfur atoms from: Cromer, D. T.; Liberman, D. J. *J. Chem. Phys.* **1970**, *53*, 1891–1898. Scattering factors for hydrogen were from: Stewart, R. F.; Davidson, E. R.; Simpson, W. T. *Ibid.* **1965**, *42*, 3175–3187.

Table I. Summary of Crystal Data and Intensity Collection Parameters

compd	$Fe(C_5Im)(TPP)(THT)\cdot C_6H_6$	$Fe(THT)_2(TPP)\cdot THT$	$[Fe(PMS)_2(TPP)]ClO_4\cdot 3CHCl_3$	$[Fe(THT)_2(TPP)]ClO_4\cdot 1.5CHCl_3$
formula	$FeSON_7C_{62}H_{54}$	$FeS_3N_4C_{56}H_{52}$	$FeCl_{10}S_2O_4N_4C_{57}H_{51}$	$FeCl_{5.5}S_2O_4N_4C_{53.5}H_{45.5}$
fw	1013.1	933.1	1330.6	1123.4
space group	$P2_1/c$	$P\bar{1}$	$P2_12_12_1$	$P\bar{1}$
a, Å	13.170 (4)[a]	13.225 (3)	17.830 (3)	13.007 (7)
b, Å	15.037 (11)	17.967 (5)	18.781 (3)	19.188 (9)
c, Å	25.422 (8)	10.283 (2)	18.187 (3)	11.256 (5)
α, deg	90.0	91.07 (2)	90.0	93.99 (3)
β, deg	90.29 (2)	99.22 (2)	90.0	107.17 (4)
γ, deg	90.0	76.59 (2)	90.0	95.01 (4)
V, Å^3	5034.4	2345.6	6090.2	2660.3
temp, °C	−175 ± 5	20 ± 1	20 ± 1	−175 ± 5
no. of reflns used for cell constants	57	56	60	60
Z	4	2	4	2
cryst dimens, mm	0.15 × 0.30 × 0.70	0.4 × 0.4 × 0.8	0.6 × 0.6 × 0.9	0.3 × 0.8 × 0.9
ρ_{calcd}, g/cm^3	1.32	1.32	1.45	1.48
ρ_{obsd}, g/cm^3	1.26[b]	1.32	1.45	1.44[b]
scan technique[c]	θ–2θ	θ–2θ	θ–2θ	ω
scan range	0.75° below $K\alpha_1$, 0.75° above $K\alpha_2$	0.8° below $K\alpha_1$, 1.0° above $K\alpha_2$	0.7 below $K\alpha_1$, 0.7 above $K\alpha_2$	0.3 centered on $K\alpha$
scan speed, deg/min	2–24	2–12	2–12	2–8
bkgds	profile analysis[d]	discrete, 0.5 times scan time	discrete, 0.5 times scan time	discrete, 0.5 times scan time
2θ range, deg	3.5–54.9	3–54.9	3–58.7	3–50.7
no. of obsd reflns	5762	7189	5778	7707
data/parameter	8.6	12.4	7.9	11.8
μ, mm^{-1}	0.35	0.45	0.74	0.63
relative transmission coeff		1.0–0.85	1.0–0.89	1.0–0.64
R_1	0.104	0.064	0.077	0.127
R_2	0.103	0.071	0.086	0.166
GOF	2.32	2.09	2.29	5.07

[a] At 20 °C, a = 13.225 (6) Å, b = 15.138 (10) Å, c = 25.652 (11) Å, and β = 90.42 (2)°. [b] All observed densities at 20 °C. [c] All experiments utilized graphite-monochromated Mo Kα radiation. [d] Blessing, R. H.; Coppen, P.; Becker, P.; *J. Appl. Crystallogr.* 1974, *7*, 488–492.

is an alternative possibility. We can only surmise that this impurity was concentrated during crystallization and may even have been responsible for the isolation of large crystals.[26] Refinement was carried to convergence by using segmented full-matrix refinement with fixed hydrogen atom contributions and anisotropic temperature factors for all heavy atoms. A final difference Fourier had a 0.8 e/Å^3 peak (about 15% of the height of a typical carbon atom) near the iron atom as the most significant feature. A listing of the final observed and calculated structure factors is available as supplementary material. Atomic coordinates and the associated anisotropic temperature factors are listed in Tables X and XI, respectively (supplementary material).

Description of the Structures. Figures 2 and 3 present perspective views of the two independent $Fe(THT)_2(TPP)$ molecules, each having required C_i—$\bar{1}$ symmetry. Individual values of the bond distances and angles in the two molecules are given in Tables XII and XIII, respectively. Figure 4 presents a formal diagram of a porphinato core displaying the perpendicular displacements, in units of 0.01 Å, of each unique atom from the mean plane of the appropriate 24-atom core. The porphinato cores of the two molecules are essentially identical and planar with the iron atom in each required by symmetry to be centered in the plane of the four nitrogen atoms. Figure 4 also presents the average values for the chemically distinct bond distances and angles. The numbers in parentheses in this diagram and subsequent diagrams presenting averages are the estimated standard deviations calculated on the assumption that the values are drawn from the same population. The phenyl rings of molecule 1 form dihedral angles of 70.9 and 89.9° and those of molecule 2 form dihedral angles of 69.9 and 72.6° with their respective mean porphinato planes.

The average Fe–N_p bond length of 1.996 (6) Å is typical for low-spin iron(II) porphyrins.[27] The most significant feature of the $Fe(THT)_2(TPP)$ molecule is the Fe(II)–S bonds. The two independent Fe(II)–S distances are essentially equivalent with values of 2.338 (1) and 2.334 (1) Å. Coordination at the sulfur atom is pyramidal, with an average C–S–C bond angle of 93.1 (3)° and an average Fe–S–C angle of 113.0 (7)°. Five-membered heterocyclic THT rings have been observed in three conformations: essentially planar, C_{2v},[28] half-chair, C_s,[29] and twisted, C_2.[30] Such rings frequently assume a number of conformations since the process is known to have relatively low interconversion barriers in the free five-membered rings. It has also been observed that these five-membered ring systems are frequently disordered, particularly at the β-carbon positions.[30] In $Fe(THT)_2(TPP)$, the relatively large thermal

Table XII. Bond Lengths in $Fe(THT)_2(TPP)\cdot THT$[a,b]

type	length, Å	type	length, Å	type	length, Å
Fe_1–N_1	2.003 (3)	Fe_2–N_3	1.990 (3)	Fe_1–S_1	2.338 (1)
Fe_1–N_2	1.992 (3)	Fe_2–N_4	1.999 (3)	Fe_2–S_2	2.334 (1)
N_1–C_{a1}	1.387 (4)	N_3–C_{a5}	1.386 (4)	S_1–C_{25}	1.817 (5)
N_1–C_{a2}	1.381 (5)	N_3–C_{a6}	1.383 (4)	S_1–C_{28}	1.819 (5)
N_2–C_{a3}	1.383 (5)	N_4–C_{a7}	1.380 (4)	S_2–C_{29}	1.827 (4)
N_2–C_{a4}	1.384 (4)	N_4–C_{a8}	1.389 (5)	S_2–C_{32}	1.829 (4)
C_{a1}–C_{b1}	1.429 (5)	C_{a5}–C_{b5}	1.435 (5)	C_{25}–C_{26}	1.447 (9)
C_{a2}–C_{b2}	1.432 (5)	C_{a6}–C_{b6}	1.429 (5)	C_{26}–C_{27}	1.409 (10)
C_{a3}–C_{b3}	1.435 (5)	C_{a7}–C_{b7}	1.442 (5)	C_{27}–C_{28}	1.500 (8)
C_{a4}–C_{b4}	1.436 (5)	C_{a8}–C_{b8}	1.439 (5)	C_{29}–C_{30}	1.521 (8)
C_{a1}–C_{m2}'	1.385 (5)	C_{a5}–C_{m3}	1.399 (5)	C_{30}–C_{31}	1.368 (10)
C_{a2}–C_{m1}	1.392 (5)	C_{a6}–C_{m4}	1.396 (5)	C_{31}–C_{32}	1.404 (8)
C_{a3}–C_{m1}	1.394 (5)	C_{a7}–C_{m4}	1.390 (5)	S_3–C_{33}	1.633 (8)
C_{a4}–C_{m2}	1.384 (5)	C_{a8}–C_{m3}'	1.385 (5)	S_3–C_{36}	1.864 (12)
C_{b1}–C_{b2}	1.341 (6)	C_{b5}–C_{b6}	1.335 (5)	C_{33}–C_{34}	1.424 (15)
C_{b3}–C_{b4}	1.337 (6)	C_{b7}–C_{b8}	1.332 (6)	C_{34}–C_{35}	1.487 (15)
C_{m1}–C_1	1.502 (5)	C_{m3}–C_{13}	1.505 (5)	C_{35}–C_{36}	1.457 (15)
C_{m2}–C_7	1.509 (5)	C_{m4}–C_{19}	1.494 (5)		

[a] The numbers in parentheses are the estimated standard deviations in the last significant figure. [b] C_i and C_i' denote atoms related by the center of inversion.

(26) We have previously found that the presence of a 1–2% H_2TPP impurity in a CoTPP sample led to the preparation of substantially larger crystals (2–10-fold) than when a rigorously pure sample was used. Moreover, the impurity level was significantly increased in the crystals (3–5-fold). Madura, P.; Scheidt, W. R., unpublished observations. These impure crystals were not used in our report of CoTPP (Madura, P.; Scheidt, W. R. *Inorg. Chem.* **1976**, *15*, 3182–3184).

(27) Scheidt, W. R. *Acc. Chem. Res.* **1977**, *10*, 339–345.

(28) Cotton, F. A.; Troup, J. M. *J. Am. Chem. Soc.* **1974**, *96*, 5070–5073.

(29) Rerat, B.; Berthold, J.; Laurent, A.; Rerat, C. *C. R. Hebd. Seances Acad. Sci., Ser. C* **1968**, *267*, 760–762.

(30) Allegra, G. Wilson, G. E., Jr.; Benedetti, E.; Pedone, C.; Albert, R. *J. Am. Chem. Soc.* **1970**, *92*, 4002–4007.

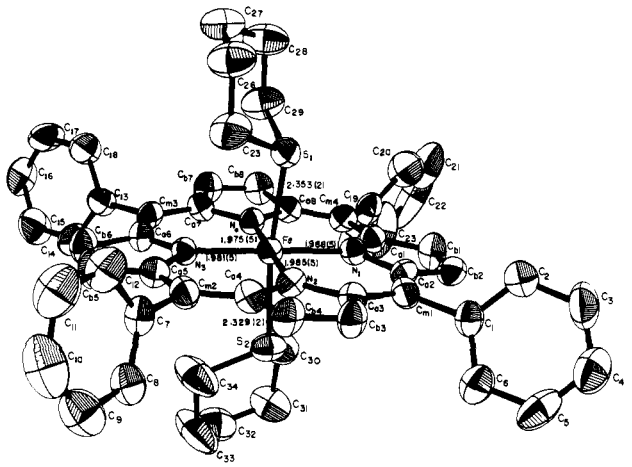

Figure 5. An ORTEP plot of the $[Fe(PMS)_2(TPP)]ClO$ molecule. The atom labels assigned to the atoms are displayed as well as the bond distances in the coordination group. All atoms are contoured at the 50% probability level.

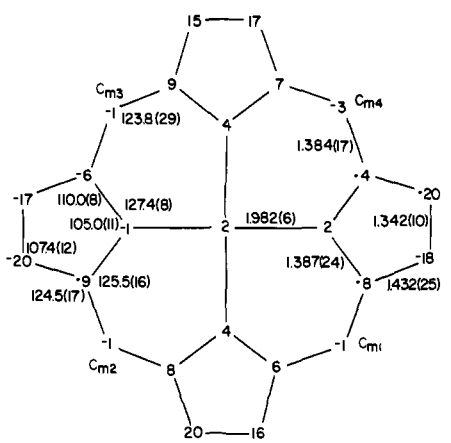

Figure 6. A formal diagram of the porphinato core of $[Fe(PMS)_2(TPP)]ClO_4$ having the same relative orientation as Figure 5. Displacements from the mean plane of the core are given in units of 0.01 Å. Averaged bond parameters are also displayed.

parameters of the β-carbons of the THT suggest that conformational change or disorder is occurring.

Figure 5 gives a computer-drawn model of the $[Fe(PMS)_2(TPP)]^+$ ion. Individual values of the bond distances and angles are presented in Tables XIV and XV, respectively, and averaged values in Figure 6. Figure 6 also displays the perpendicular displacement of the atoms from the mean plane of the core. Although there is no required symmetry of the $[Fe(PMS)_2(TPP)]^+$ moiety in the crystal, the pattern of displacements conforms closely to that which would be required by D_{2d} symmetry. The iron(III) atom is only very slightly displaced out of the center of the macrocycle. The four phenyl rings form dihedral angles of 63.3, 74.4, 82.5, and 63.9° with the mean plane of the core.

The averaged $Fe-N_p$ distance of 1.982 (6) Å is essentially equal to the 1.990-Å value expected[27] for low-spin iron(III)-porphyrin complexes. The two independent Fe(III)-S distances are 2.353 (2) and 2.329 (2) Å; i.e., one distance is slightly shorter than that in the *iron(II) complex* and the other slightly longer. Similar nonequivalent Fe(III)-S distances are found in $[Fe(THT)_2(TPP)]^+$. The S_1-Fe-S_2 angle is 171.1 (1)°, and the Fe(III)-S vectors are 3.2 and 5.6° from being normal to the mean plane of the core. This is similar to the geometry displayed by the two $Fe(THT)_2(TPP)$ molecules. While the symmetry of $Fe(THT)_2(TPP)$ requires that the S-Fe-S′ group in each molecule be linear; the Fe(II)-S vectors are 3.9 and 4.2° from the heme normal in molecules 1 and 2, respectively.

The pentamethylene sulfide ligands in $[Fe(PMS)_2(TPP)]^+$ are ordered. The six-membered rings are in the chair conformation. The dihedral angles between the C-S-C plane and the 4-carbon plane are 50.5 and 49.8°. The two 3-atom end planes (C-S-C and C-C-C) are almost parallel with an average diedral angle of 1.5°. The coordination at sulfur is again pyramidal with an average Fe-S-C angle of 110.6 (2)° and C-S-C angles of 99.4 (7)°. The C-S-C angles are similar to those observed in other six-membered sulfur heterocycles.[31,32]

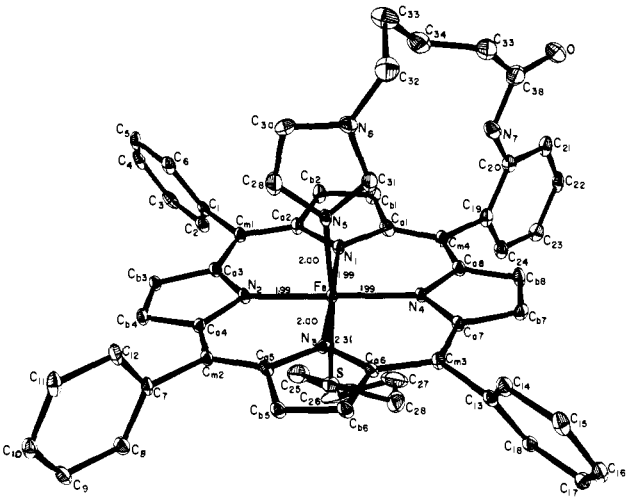

Figure 7. A computer-produced perspective view of the $Fe(\overline{C5Im})(\overline{TPP})(THT)$ molecule using 50% probability ellipsoids. The labels assigned to each atom are shown as are the distances around the iron(II) atom.

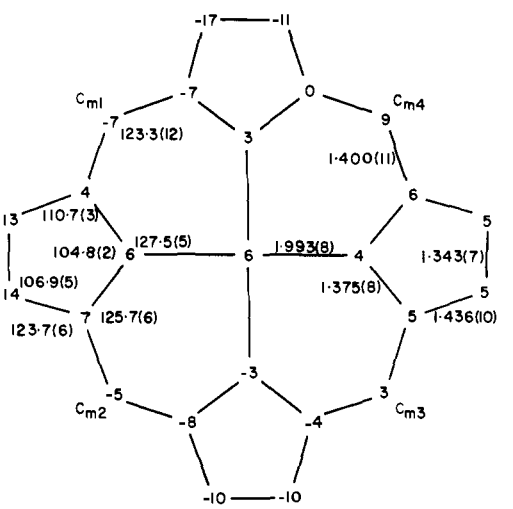

Figure 8. A formal diagram of the porphinato core of the $Fe(\overline{C5Im})(\overline{TPP})(THT)$ molecule. The core has the same relative orientation as that of Figure 7. Averaged bond parameters are shown along with the perpendicular displacements, in units of 0.01 Å, from the mean plane of the porphinato core.

Figure 7 exhibits the structure of the $Fe(\overline{C5Im})(\overline{TPP})(THT)$ molecule as it exists in the crystal. Bond distances in the coordination group are also displayed in the figure. Individual values for distances and angles are presented in Tables XVI and XVII and averaged values in Figure 8. This figure also displays the perpendicular displacements of the atoms from the mean plane of the 24-atom core. The pattern of displacements corresponds closely to that required for a modest D_{2d} type of ruffling. The 0.06-Å displacement of the iron(II) is toward the attached imidazole ligand. The dihedral angles between the mean plane of the core and the three unsubstituted phenyl groups are 67.5, 84.4, and 65.2°. The corresponding angle for the phenyl group bearing the tail substituent is 87.9°, showing it to be somewhat closer to being perpendicular than average, but not outside the observed range. The atoms of the valeramido bridge between the imidazole ligand and the phenyl group appear to be well-ordered, at least at low temperature, with normal values for the bonding parameters.

The average $Fe-N_p$ distance is a normal low-spin iron(II) value of 1.993 (8) Å. The Fe-N distance to the tail imidazole ligand is 2.004 (5)

(31) Cotton, F. A.; Kolb, J. R.; Stults, B. R. *Inorg. Chim. Acta* **1975**, *15*, 239-244.

(32) Costello, W. R.; McPhail, A. T.; Sim, G. A. *J. Chem. Soc. A* **1966**, 1190-1193. Knobler, C.; Hope, H.; McCullough, J. D. *Inorg. Chem.* **1971**, *10*, 697-700. Marsh, R. E. *Acta Crystallogr.* **1955**, *8*, 91-94. Valle, G.; Busetti, V.; Mammi, M.; Carazzolo, G. *Acta Crystallogr., Sect. B* **1969**, *B25*, 1432-1436.

Table XIII. Bond Angles in $Fe(THT)_2(TPP)\cdot THT$[a,b]

type	angle, deg	type	angle, deg	type	angle, deg
$N_1Fe_1N_2$	89.7 (1)	$N_3Fe_2N_4$	89.8 (1)	$C_{a1}C_{m2}C_7$	118.1 (3)
$N_1Fe_1S_1$	88.7 (1)	$N_3Fe_2S_2$	91.7 (1)	$C_{a4}C_{m2}C_7$	117.2 (3)
$N_1Fe_1S_1$	86.7 (1)	$N_4Fe_2S_2$	86.3 (1)	$C_{a2}C_{m1}C_1$	118.8 (3)
$Fe_1N_1C_{a1}$	126.8 (2)	$Fe_2N_3C_{a5}$	127.5 (2)	$C_{a3}C_{m1}C_1$	117.5 (3)
$Fe_1N_1C_{a2}$	127.5 (2)	$Fe_2N_3C_{a6}$	127.9 (2)	$C_{a1}C_{m2}C_{a4}$	124.8 (3)
$Fe_1N_2C_{a3}$	127.7 (2)	$Fe_2N_4C_{a7}$	127.4 (2)	$C_{a2}C_{m1}C_{a3}$	123.6 (3)
$Fe_1N_2C_{a4}$	127.0 (2)	$Fe_2N_4C_{a8}$	127.1 (2)	$C_{a5}C_{m3}C_{13}$	117.0 (3)
$Fe_1S_1C_{25}$	112.7 (2)	$Fe_2S_2C_{29}$	112.5 (1)	$C_{a8}'C_{m3}C_{13}$	118.8 (3)
$Fe_1S_1C_{28}$	114.1 (2)	$Fe_2S_2C_{32}$	112.7 (1)	$C_{a6}C_{m4}C_{19}$	118.0 (3)
$C_{a1}N_1C_{a2}$	105.5 (3)	$C_{a5}N_3C_{a6}$	104.6 (3)	$C_{a7}C_{m4}C_{19}$	118.2 (3)
$C_{a3}N_2C_{a4}$	105.2 (3)	$C_{a7}N_4C_{a8}$	105.5 (3)	$C_{a5}C_{m3}C_{a8}'$	124.1 (3)
$N_1C_{a1}C_{m2}$	125.4 (3)	$N_3C_{a5}C_{m3}$	125.3 (3)	$C_{a6}C_{m4}C_{a7}$	123.7 (3)
$N_1C_{a2}C_{m1}$	125.6 (3)	$N_3C_{a6}C_{m4}$	125.3 (3)	$C_{25}S_1C_{28}$	92.9 (2)
$N_2C_{a3}C_{m1}$	125.6 (3)	$N_4C_{a7}C_{m4}$	125.9 (3)	$S_1C_{25}C_{26}$	106.3 (4)
$N_2C_{a4}C_{m2}$	125.6 (3)	$N_4C_{a8}C_{m3}'$	125.7 (3)	$C_{25}C_{26}C_{27}$	113.4 (5)
$N_1C_{a1}C_{b1}$	109.3 (3)	$N_3C_{a5}C_{b5}$	110.1 (3)	$C_{26}C_{27}C_{28}$	110.5 (5)
$N_1C_{a2}C_{b2}$	110.1 (3)	$N_3C_{a6}C_{b6}$	110.5 (3)	$C_{27}C_{28}S_1$	107.3 (4)
$N_2C_{a3}C_{b3}$	109.8 (3)	$N_4C_{a7}C_{b7}$	109.6 (3)	$C_{29}S_2C_{32}$	93.3 (2)
$N_2C_{a4}C_{b4}$	110.0 (3)	$N_4C_{a8}C_{b8}$	109.6 (3)	$S_2C_{29}C_{30}$	106.5 (4)
$C_{m2}C_{a1}C_{b1}$	125.3 (3)	$C_{m3}C_{a5}C_{b5}$	124.6 (3)	$C_{29}C_{30}C_{31}$	112.7 (5)
$C_{m1}C_{a2}C_{b2}$	124.3 (3)	$C_{m4}C_{a6}C_{b6}$	124.2 (3)	$C_{30}C_{31}C_{32}$	119.5 (5)
$C_{m1}C_{a3}C_{b3}$	124.6 (3)	$C_{m4}C_{a7}C_{b7}$	124.5 (3)	$C_{31}C_{32}S_2$	107.4 (4)
$C_{m2}C_{a4}C_{b4}$	124.3 (3)	$C_{m3}'C_{a8}C_{b8}$	124.7 (3)	$C_{33}S_3C_{36}$	95.2 (4)
$C_{a1}C_{b1}C_{b2}$	108.2 (3)	$C_{a5}C_{b5}C_{b6}$	107.4 (3)	$S_3C_{33}C_{34}$	110.0 (6)
$C_{a2}C_{b2}C_{b1}$	106.9 (3)	$C_{a6}C_{b6}C_{b5}$	107.4 (3)	$C_{33}C_{34}C_{35}$	114.5 (7)
$C_{a3}C_{b3}C_{b4}$	107.7 (3)	$C_{a7}C_{b7}C_{b8}$	107.8 (3)	$C_{34}C_{35}C_{36}$	105.9 (8)
$C_{a4}C_{b4}C_{b3}$	107.2 (3)	$C_{a8}C_{b8}C_{b7}$	107.5 (3)	$C_{35}C_{36}S_3$	105.2 (7)

[a] The numbers in parentheses are the estimated standard deviations in the last significant figure. [b] C_i and C_i' denote atoms related by the center of inversion.

Table XIV. Bond Lengths in $[Fe(PMS)_2(TPP)]^+$[a]

type	length, Å	type	length, Å	type	length, Å
$Fe-S_1$	2.353 (2)	$C_{m1}-C_1$	1.533 (10)	$C_{11}-C_{12}$	1.377 (12)
$Fe-S_2$	2.329 (2)	$C_{m2}-C_7$	1.523 (10)	$C_{12}-C_7$	1.369 (11)
$Fe-N_1$	1.988 (5)	$C_{m3}-C_{13}$	1.505 (10)	$C_{13}-C_{14}$	1.357 (11)
$Fe-N_2$	1.985 (5)	$C_{m4}-C_{19}$	1.443 (10)	$C_{14}-C_{15}$	1.375 (12)
$Fe-N_3$	1.981 (5)	S_1-C_{25}	1.808 (9)	$C_{15}-C_{16}$	1.354 (13)
$Fe-N_4$	1.975 (5)	S_1-C_{29}	1.817 (9)	$C_{16}-C_{17}$	1.359 (13)
N_1-C_{a1}	1.351 (9)	S_2-C_{30}	1.786 (9)	$C_{17}-C_{18}$	1.366 (11)
N_1-C_{a2}	1.425 (8)	S_2-C_{34}	1.786 (10)	$C_{18}-C_{13}$	1.383 (11)
N_2-C_{a3}	1.405 (8)	$C_{25}-C_{26}$	1.521 (13)	$C_{19}-C_{20}$	1.394 (13)
N_2-C_{a4}	1.389 (8)	$C_{26}-C_{27}$	1.446 (13)	$C_{20}-C_{21}$	1.426 (14)
N_3-C_{a5}	1.405 (8)	$C_{27}-C_{28}$	1.521 (13)	$C_{21}-C_{22}$	1.312 (25)
N_3-C_{a6}	1.360 (8)	$C_{28}-C_{29}$	1.521 (13)	$C_{22}-C_{23}$	1.331 (25)
N_4-C_{a7}	1.379 (8)	$C_{30}-C_{31}$	1.533 (13)	$C_{23}-C_{24}$	1.367 (14)
N_4-C_{a8}	1.379 (9)	$C_{31}-C_{32}$	1.423 (13)	$C_{24}-C_{19}$	1.404 (13)
$C_{m1}-C_{a2}$	1.356 (10)	$C_{32}-C_{33}$	1.532 (17)	Cl_1-O_1	1.360 (10)
$C_{m1}-C_{a3}$	1.409 (10)	$C_{33}-C_{34}$	1.529 (14)	Cl_1-O_2	1.420 (7)
$C_{m2}-C_{a4}$	1.368 (10)	$C_{b1}-C_{b2}$	1.357 (13)	Cl_1-O_3	1.398 (9)
$C_{m2}-C_{a5}$	1.381 (10)	$C_{b3}-C_{b4}$	1.339 (10)	Cl_1-O_4	1.372 (9)
$C_{m3}-C_{a6}$	1.397 (10)	$C_{b5}-C_{b6}$	1.335 (10)	$C_{35}-Cl_2$	1.760 (11)
$C_{m3}-C_{a7}$	1.377 (10)	$C_{b7}-C_{b8}$	1.335 (10)	$C_{35}-Cl_3$	1.740 (11)
$C_{m4}-C_{a8}$	1.392 (10)	C_1-C_2	1.359 (11)	$C_{35}-Cl_4$	1.769 (12)
$C_{m4}-C_{a1}$	1.396 (10)	C_2-C_3	1.414 (11)	$C_{36}-Cl_5$	1.764 (14)
$C_{a1}-C_{b1}$	1.456 (10)	C_3-C_4	1.320 (13)	$C_{36}-Cl_6$	1.714 (14)
$C_{a2}-C_{b2}$	1.398 (10)	C_4-C_5	1.317 (13)	$C_{36}-Cl_7$	1.661 (14)
$C_{a3}-C_{b3}$	1.408 (10)	C_5-C_6	1.393 (11)	$C_{37}-Cl_8$	1.749 (13)
$C_{a4}-C_{b4}$	1.429 (10)	C_6-C_1	1.380 (11)	$C_{37}-Cl_9$	1.763 (13)
$C_{a5}-C_{b5}$	1.413 (10)	C_7-C_8	1.350 (11)	$C_{37}-Cl_{10}$	1.685 (14)
$C_{a6}-C_{b6}$	1.434 (10)	C_8-C_9	1.386 (11)	$C_{37}-Cl_{11}$	1.671 (15)
$C_{a7}-C_{b7}$	1.467 (10)	C_9-C_{10}	1.362 (14)	$C_{37}-Cl_{12}$	1.682 (13)
$C_{a8}-C_{b8}$	1.454 (10)	$C_{10}-C_{11}$	1.382 (14)	$C_{37}-Cl_{13}$	1.862 (14)

[a] The number in parentheses is the estimated standard deviation in the last significant figure.

Å, and the imidazole ligand is planar to within ±0.01 Å. The angle between the normal to the imidazole plane and the normal to the heme plane is 85°. The iron(II) atom is displaced 0.13 Å from the imidazole plane. The Fe–N(Im) vector is tipped 2.4° from the normal to the core. Similar off-axis distortions have been found in other imidazole adducts of metalloporphyrins[33] and imidazole complexes.[34] The dihedral angle formed by the imidazole plane and the coordination planes containing N_2 or N_4 is 3.5°. This angle, frequently noted as ϕ, is a measure of the nonbonded interactions between an axial planar ligand and the porphyrin core; such interactions are maximized at $\phi = 0$ and minimized at $\phi = 45°$. The Fe(II)–S distance is 2.307 (3) Å. The N_3–Fe–S angle is nonlinear at 173.8 (2)°. As in the other thioether derivatives, the Fe(II)–S vector is not perpendicular to the heme plane but is tilted 7° from the normal. The THT ligand displays similar coordination properties in Fe(C5Im)(TPP)(THT) as in $Fe(THT)_2(TPP)$ and similarly the five-membered ring has a C_2 twisted conformation.

Discussion

Synthetic Aspects. The mixed axial ligation in cytochrome *c* provided by histidine and methionine poses an immediate problem for the synthesis of an active site analogue. The greater affinity of heme iron for imidazole compared to thioethers, particularly in the ferric state, means that success with self-assembly synthesis is most unlikely. However, the "tail porphyrin" strategy, whose first successful application was with spectrally detectable cytochrome *c* models,[11-13] is well suited to dictating the coordination of a single imidazole. A number of hemoglobin models exploit the same concept.[16,21,35] Intent on isolating a pure crystalline solid, numerous attempts were made with various thioethers and varied imidazole tail lengths until the crystalline ferrocytochrome *c* analogue, Fe(C5Im)(TPP)(THT)·C_6C_6 (**1**), was isolated (see Figure 7). Obtaining a single crystal and determining its X-ray crystal structure represents the first time a tail porphyrin has been thus characterized.[36] More frequently, powders resulted from crystal growing attempts with the tail porphyrin complexes. This, together with the all too probable difficulties of methylene group disorder, illustrates a significant limitation to the tail porphyrin approach. A more symmetrical, doubly-attached, ligand bridge is likely to be better suited to isolating crystalline complexes. Furthermore, the problem of "nose-to-tail" dimers[16] is a significant one and appears to prevent us from isolating an analogous *ferricytochrome c* model with the present tail porphyrin.

(33) Kirner, J. F.; Reed, C. A.; Scheidt, W. R. *J. Am. Chem. Soc.* **1977**, *99*, 2557–2563 and references therein.

(34) Freeman, H. C. *Adv. Protein Chem.* **1967**, *22*, 308–424.

(35) Geibel, J.; Cannon, J.; Campbell, D.; Traylor, T. G. *J. Am. Chem. Soc.* **1978**, *100*, 3575–3585.

(36) Since the completion of this work, the crystal structure of a five-coordinate zinc complex with a pyridine "tail" has appeared: Bobrick, M. A.; Walker, F. A. *Inorg. Chem.* **1980**, *19*, 3383–3390.

Table XV. Bond Angles in $[Fe(PMS)_2(TPP)]^+$ [a]

type	angle, deg	type	angle, deg
S_1FeS_2	171.1 (1)	$C_{a2}C_{m1}C_1$	117.6 (6)
N_1FeN_2	91.0 (2)	$C_{a3}C_{m1}C_1$	115.6 (6)
N_1FeN_3	179.0 (12)	$C_{a4}C_{m2}C_7$	117.7 (6)
N_1FeN_4	89.1 (2)	$C_{a5}C_{m2}C_7$	116.7 (6)
N_2FeN_3	89.5 (2)	$C_{a6}C_{m3}C_{13}$	118.9 (6)
N_2FeN_4	178.9 (15)	$C_{a7}C_{m3}C_{13}$	118.2 (6)
N_3FeN_4	90.5 (2)	$C_{a8}C_{m4}C_{19}$	120.7 (7)
S_1FeN_1	87.5 (2)	$C_{a1}C_{m4}C_{19}$	119.1 (7)
S_1FeN_2	87.3 (2)	$N_1C_{a1}C_{m4}$	127.3 (7)
S_1FeN_3	93.4 (2)	$N_1C_{a2}C_{m1}$	124.4 (6)
S_1FeN_4	91.5 (2)	$N_2C_{a3}C_{m1}$	123.4 (6)
S_2FeN_1	86.3 (2)	$N_2C_{a4}C_{m2}$	123.8 (6)
S_2FeN_2	86.3 (2)	$N_3C_{a5}C_{m2}$	124.8 (7)
S_2FeN_3	92.8 (2)	$N_3C_{a6}C_{m3}$	125.7 (6)
S_2FeN_4	94.8 (2)	$N_4C_{a7}C_{m3}$	126.9 (6)
FeS_1C_{25}	110.6 (3)	$N_4C_{a8}C_{m4}$	127.6 (6)
FeS_1C_{29}	110.4 (3)	$C_{b1}C_{a1}C_{m4}$	121.5 (7)
FeS_2C_{30}	110.5 (3)	$C_{b2}C_{a2}C_{m1}$	125.9 (7)
FeS_2C_{34}	110.8 (3)	$C_{b3}C_{a3}C_{m1}$	126.3 (6)
FeN_1C_{a1}	128.2 (5)	$C_{b4}C_{a4}C_{m2}$	125.5 (7)
FeN_1C_{a2}	126.6 (4)	$C_{b5}C_{a5}C_{m2}$	126.1 (7)
FeN_2C_{a3}	127.5 (5)	$C_{b6}C_{a6}C_{m3}$	123.7 (6)
FeN_2C_{a4}	128.8 (4)	$C_{b7}C_{a7}C_{m3}$	123.7 (6)
FeN_3C_{a5}	127.2 (5)	$C_{b8}C_{a8}C_{m4}$	123.1 (6)
FeN_3C_{a6}	127.5 (5)	$C_{25}C_{26}C_{27}$	116.7 (8)
FeN_4C_{a7}	126.2 (4)	$C_{26}C_{27}C_{28}$	113.7 (8)
FeN_4C_{a8}	127.3 (4)	$C_{27}C_{28}C_{29}$	112.3 (7)
$S_1C_{25}C_{26}$	110.6 (7)	$C_{30}C_{31}C_{32}$	114.4 (8)
$S_1C_{29}C_{28}$	109.6 (6)	$C_{31}C_{32}C_{33}$	113.1 (9)
$S_2C_{30}C_{31}$	111.0 (6)	$C_{32}C_{33}C_{34}$	115.0 (11)
$S_2C_{34}C_{33}$	109.6 (7)	$O_1Cl_1O_2$	116.7 (6)
$C_{25}S_1C_{29}$	98.9 (4)	$O_1Cl_1O_3$	105.4 (8)
$C_{30}S_2C_{34}$	99.9 (5)	$O_1Cl_1O_4$	109.8 (8)
$C_{a1}N_1C_{a2}$	104.8 (5)	$O_2Cl_1O_3$	110.5 (6)
$C_{a3}N_2C_{a4}$	103.7 (5)	$O_2Cl_1O_4$	110.8 (5)
$C_{a5}N_3C_{a6}$	105.2 (5)	$O_3Cl_1O_4$	102.5 (7)
$C_{a7}N_4C_{a8}$	106.5 (5)	$Cl_2C_{35}Cl_3$	109.7 (6)
$N_1C_{a1}C_{b1}$	111.3 (6)	$Cl_2C_{35}Cl_4$	108.2 (6)
$N_1C_{a2}C_{b2}$	109.7 (6)	$Cl_3C_{35}Cl_4$	109.6 (7)
$N_2C_{a3}C_{b3}$	110.3 (6)	$Cl_5C_{36}Cl_4$	104.7 (7)
$N_2C_{a4}C_{b4}$	110.7 (6)	$Cl_5C_{36}Cl_6$	109.2 (8)
$N_3C_{a5}C_{b5}$	109.0 (6)	$Cl_6C_{36}Cl_7$	113.6 (8)
$N_3C_{a6}C_{b6}$	110.6 (6)	$Cl_8C_{37}Cl_7$	104.0 (7)
$N_4C_{a7}C_{b7}$	109.3 (6)	$Cl_8C_{37}Cl_9$	110.4 (7)
$N_4C_{a8}C_{b8}$	109.4 (6)	$Cl_9C_{37}Cl_{10}$	112.2 (8)
$C_{a1}C_{b1}C_{b2}$	105.4 (7)	$Cl_{11}C_{37}Cl_{12}$	111.3 (8)
$C_{a2}C_{b2}C_{b1}$	108.9 (7)	$Cl_{11}C_{37}Cl_{13}$	101.8 (8)
$C_{a3}C_{b3}C_{b4}$	108.4 (6)	$Cl_{12}C_{37}Cl_{13}$	105.7 (8)
$C_{a4}C_{b4}C_{b3}$	106.8 (7)	$C_{a6}C_{b6}C_5$	106.7 (7)
$C_{a5}C_{b5}C_{b6}$	108.6 (7)	$C_{a7}C_{b7}C_8$	106.9 (7)
$C_{a8}C_{b8}C_{b7}$	107.9 (7)	$C_{a6}C_{m3}C_{a7}$	122.8 (6)
$C_{a2}C_{m1}C_{a3}$	126.7 (7)	$C_{a8}C_{m4}C_{a1}$	120.2 (6)
$C_{a4}C_{m2}C_{a5}$	125.5 (7)		

[a] The numbers in parentheses are the estimated standard deviations in the last significant figure.

Table XVI. Interatomic Distances (Å) for $Fe(C_5Im)(TPP)(THT)\cdot C_6H_6$

$Fe-Fe_2$	0.53	$C_{a7}-C_{m3}$	1.403 (8)	$C_{16}-C_{17}$	1.375 (10)
$Fe-N_1$	1.992 (5)	$C_{a7}-C_{b7}$	1.428 (8)	$C_{17}-C_{18}$	1.394 (9)
$Fe-N_2$	1.988 (5)	$C_{a8}-C_{m4}$	1.410 (9)	$C_{m4}-C_{19}$	1.531 (8)
$Fe-N_3$	2.004 (5)	$C_{a8}-C_{b8}$	1.417 (9)	$C_{19}-C_{20}$	1.393 (10)
$Fe-N_4$	1.987 (5)	$C_{b1}-C_{b2}$	1.341 (9)	$C_{19}-C_{24}$	1.354 (10)
Fe-S	2.307 (3)	$C_{b3}-C_{b4}$	1.344 (8)	$C_{20}-C_{21}$	1.406 (9)
$Fe-N_5$	2.002 (7)	$C_{b5}-C_{b6}$	1.335 (8)	$C_{20}-N_7$	1.397 (10)
Fe_2-Br	2.32	$C_{b7}-C_{b8}$	1.353 (9)	$C_{21}-C_{22}$	1.388 (12)
N_1-C_{a1}	1.374 (8)	$C_{m1}-C_1$	1.491 (8)	$C_{22}-C_{23}$	1.380 (11)
N_1-C_{a2}	1.372 (8)	C_1-C_2	1.365 (9)	$C_{23}-C_{24}$	1.376 (10)
N_2-C_{a3}	1.379 (7)	C_1-C_6	1.398 (10)	$S-C_{25}$	1.779 (11)
N_2-C_{a4}	1.377 (7)	C_2-C_3	1.397 (10)	$S-C_{28}$	1.762 (11)
N_3-C_{a5}	1.384 (7)	C_3-C_4	1.352 (11)	$C_{25}-C_{26}$	1.525 (16)
N_3-C_{a6}	1.358 (7)	C_4-C_5	1.363 (11)	$C_{26}-C_{27}$	1.496 (20)
N_4-C_{a7}	1.376 (7)	C_5-C_6	1.376 (9)	$C_{27}-C_{28}$	1.417 (18)
N_4-C_{a8}	1.379 (7)	$C_{m2}-C_7$	1.499 (8)	N_5-C_{29}	1.342 (11)
$C_{a1}-C_{m4}$	1.380 (9)	C_7-C_8	1.381 (9)	N_5-C_{31}	1.291 (10)
$C_{a1}-C_{b1}$	1.442 (9)	C_7-C_{12}	1.366 (10)	$C_{29}-C_{30}$	1.310 (12)
$C_{a2}-C_{m1}$	1.406 (8)	C_8-C_9	1.392 (9)	$C_{30}-N_6$	1.327 (10)
$C_{a2}-C_{b2}$	1.445 (8)	C_9-C_{10}	1.328 (10)	$C_{31}-N_6$	1.334 (10)
$C_{a3}-C_{m1}$	1.402 (8)	$C_{10}-C_{11}$	1.382 (10)	N_6-C_{32}	1.427 (12)
$C_{a3}-C_{b3}$	1.433 (8)	$C_{11}-C_{12}$	1.416 (9)	$C_{32}-C_{33}$	1.552 (14)
$C_{a4}-C_{m2}$	1.402 (8)	$C_{m3}-C_{13}$	1.492 (8)	$C_{33}-C_{34}$	1.530 (14)
$C_{a4}-C_{b4}$	1.444 (8)	$C_{13}-C_{14}$	1.364 (9)	$C_{34}-C_{35}$	1.497 (14)
$C_{a5}-C_{m2}$	1.385 (8)	$C_{13}-C_{18}$	1.401 (9)	$C_{35}-C_{36}$	1.523 (14)
$C_{a5}-C_{b5}$	1.433 (8)	$C_{14}-C_{15}$	1.396 (9)	$C_{36}-N_7$	1.386 (12)
$C_{a6}-C_{m3}$	1.411 (8)	$C_{15}-C_{16}$	1.364 (10)	$C_{36}-O$	1.225 (10)
$C_{a6}-C_{b6}$	1.445 (8)				

Scheme I. Probable Equilibria for $Fe(C_5Im)(TPP)(ClO_4)$

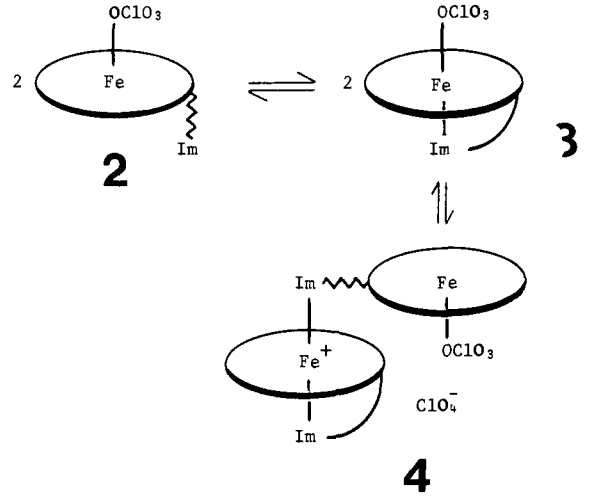

In solution, the equilibria of Scheme I define the probable species for the precursor complex $Fe(C5Im)(TPP)(ClO_4)$. The EPR spectrum of a frozen dichloromethane/chloroform solution (10 K) suggests that species **4** predominates since both low-spin (g = 2.86, 2.28, 1.58) and high-spin (g = 5.90, 1.99) signals are observed (see Figure 9a). These values compare favorably with those of low-spin $[Fe(HIm)(C5Im)(TPP)]ClO_4$ (g = 2.90, 2.30, 1.68; Figure 9b) and high-spin $Fe(OClO_3)(TPP)$ (g = 5.85, 1.98).[37] Upon isolation of a solid (powder), the nose-to-tail dimer, **4**, is again the probable predominant species as judged by the magnetic moment (μ = 4.5 μ_B). This value is in the range expected from a 1:1 mixture of low spin (μ = 2.3 μ_B) and admixed intermediate (μ = 5.2 μ_B) or high-spin (μ = 5.9 μ_B) species. Similarly, the chloride analogue has μ = 4.7 μ_B. When an excess of a thioether such as PMS is added to **4**, a low-spin EPR spectrum is obtained (Figure 9c). We ascribe this EPR spectrum to a ferricytochrome c analogue $[Fe(C5Im)(TPP)(PMS)]ClO_4$ since its g values of 2.90, 2.37 and 1.48 are distinguishable from a mixture of bis(imidazole) (g = 2.86, 2.28, 1.58; Figure 9a) and bis(thioether) (g = 2.91, 2.37) species (Figure 9d). However, all attempts to crystallize this species gave powders with higher than expected magnetic moments and inconsistent elemental analyses.

The congruence between the EPR of cytochrome c (g = 3.06, 2.25, and 1.25)[38] and the model (g = 2.90, 2.37, and 1.48) is qualitatively in the right direction since the spread of g values is greater than for bis(imidazole) derivatives. Methionine/histidine-ligated cytochromes typically have higher g_1 and lower g_3 values than bis(histidine) ligated cytochromes.[38] A quantitative correlation of g values should perhaps not be expected since there is an inherent asymmetry to the sp^3 sulfur donor atom[39] and

(37) $Fe(OClO_3)(TPP)$ gives high-spin EPR spectra in frozen 2-MeTHF solution but appears to be a quantum mechanically admixed intermediate (S = $^5/_2$, $^3/_2$) state in the solid form (see ref 22).

(38) Brautigan, D. L.; Feinberg, B. A.; Hoffman, B. M.; Margoliash, E.; Peisach, J.; Blumberg, W. E. *J. Biol. Chem.* **1977**, *252*, 574–582.
(39) Senn, H.; Keller, R. M.; Wuthrick, K. *Biochem. Biophys. Res. Commun.* **1980**, *92*, 1362–1369.

Table XVII. Bond Angles (Deg) for Fe(C$_5$Im)(TPP)(THT)·C$_6$H$_6$

N_1-Fe-N_2	89.97 (20)	C_{a5}-C_{m2}-C_7	117.4 (5)
N_1-Fe-N_3	176.19 (23)	C_{a6}-C_{m3}-C_{13}	119.8 (6)
N_1-Fe-N_4	90.61 (21)	C_{a7}-C_{m3}-C_{13}	118.2 (6)
N_1-Fe-N_5	87.58 (24)	C_{a8}-C_{m4}-C_{19}	118.5 (6)
N_2-Fe-N_3	90.11 (20)	C_{m1}-C_1-C_2	123.8 (7)
N_2-Fe-N_4	178.77 (25)	C_{m1}-C_1-C_6	118.8 (6)
N_2-Fe-N_5	89.30 (24)	C_6-C_1-C_2	117.3 (7)
N_3-Fe-N_4	89.23 (20)	C_1-C_2-C_3	121.7 (8)
N_3-Fe-N_5	88.61 (23)	C_2-C_3-C_4	118.5 (7)
N_4-Fe-N_5	89.64 (24)	C_3-C_4-C_5	122.3 (7)
Fe-N_1-C_{a1}	127.2 (4)	C_4-C_5-C_6	118.4 (8)
Fe-N_1-C_{a2}	127.9 (4)	C_5-C_6-C_1	121.7 (7)
Fe-N_2-C_{a3}	127.4 (4)	C_{m2}-C_7-C_8	122.0 (6)
Fe-N_2-C_{a4}	127.9 (4)	C_{m2}-C_7-C_{12}	119.6 (6)
Fe-N_3-C_{a5}	126.9 (4)	C_{12}-C_7-C_8	118.3 (6)
Fe-N_3-C_{a6}	127.9 (4)	C_7-C_8-C_9	119.9 (7)
Fe-N_4-C_{a7}	128.2 (4)	C_8-C_9-C_{10}	121.8 (7)
Fe-N_4-C_{a8}	126.9 (4)	C_9-C_{10}-C_{11}	120.4 (6)
C_{a1}-N_1-C_{a2}	104.7 (5)	C_{10}-C_{11}-C_{12}	118.1 (7)
C_{a3}-N_2-C_{a4}	104.7 (5)	C_{11}-C_{12}-C_7	121.4 (7)
C_{a5}-N_3-C_{a6}	105.1 (5)	C_{m3}-C_{13}-C_{18}	122.3 (7)
C_{a7}-N_4-C_{a8}	104.8 (5)	C_{m3}-C_{13}-C_{14}	119.2 (6)
N_1-C_{a1}-C_{m4}	125.5 (6)	C_{18}-C_{13}-C_{14}	118.5 (6)
N_1-C_{a1}-C_{b1}	110.4 (6)	C_{13}-C_{14}-C_{15}	121.6 (7)
C_{m4}-C_{a1}-C_{b1}	124.0 (6)	C_{14}-C_{15}-C_{16}	119.5 (7)
N_1-C_{a2}-C_{m1}	125.6 (6)	C_{15}-C_{16}-C_{17}	120.4 (7)
N_1-C_{a2}-C_{b2}	111.3 (6)	C_{16}-C_{17}-C_{18}	120.1 (7)
C_{m1}-C_{a2}-C_{b2}	123.0 (6)	C_{17}-C_{18}-C_{13}	119.9 (7)
N_2-C_{a3}-C_{m1}	126.2 (6)	C_{m4}-C_{19}-C_{20}	120.6 (7)
N_2-C_{a3}-C_{b3}	110.7 (5)	C_{m4}-C_{19}-C_{24}	119.3 (7)
C_{m1}-C_{a3}-C_{b3}	123.2 (6)	C_{24}-C_{19}-C_{20}	120.1 (7)
N_2-C_{a4}-C_{m2}	124.7 (6)	C_{19}-C_{20}-C_{21}	119.3 (8)
N_2-C_{a4}-C_{b4}	110.6 (5)	C_{19}-C_{20}-N_7	116.9 (7)
C_{m2}-C_{a4}-C_{b4}	124.6 (6)	C_{21}-C_{20}-N_7	123.8 (8)
N_3-C_{a5}-C_{m2}	125.6 (6)	C_{20}-C_{21}-C_{22}	118.6 (8)
N_3-C_{a5}-C_{b5}	110.3 (5)	C_{21}-C_{22}-C_{23}	121.6 (7)
C_{m2}-C_{a5}-C_{b5}	124.1 (6)	C_{22}-C_{23}-C_{24}	118.3 (8)
N_3-C_{a6}-C_{m3}	126.5 (6)	C_{23}-C_{24}-C_{25}	122.2 (8)
N_3-C_{a6}-C_{b6}	110.5 (5)	Fe-S-C_{25}	110.3 (4)
C_{m3}-C_{a6}-C_{b6}	123.0 (6)	Fe-S-C_{28}	114.4 (4)
N_4-C_{a7}-C_{m3}	126.0 (6)	C_{28}-S-C_{25}	92.4 (6)
N_4-C_{a7}-C_{b7}	110.4 (5)	S-C_{25}-C_{26}	105.1 (9)
C_{m3}-C_{a7}-C_{b7}	123.6 (6)	S-C_{28}-C_{27}	109.3 (9)
N_4-C_{a8}-C_{m4}	125.2 (6)	C_{25}-C_{26}-C_{27}	106.0 (11)
N_4-C_{a8}-C_{b8}	111.0 (6)	C_{26}-C_{27}-C_{28}	103.1 (11)
C_{m4}-C_{a8}-C_{b8}	123.8 (6)	Fe-N_5-C_{29}	127.8 (6)
C_{a1}-C_{b1}-C_{b2}	107.6 (6)	Fe-N_5-C_{31}	130.0 (6)
C_{a2}-C_{b2}-C_{b1}	105.9 (6)	C_{29}-N_5-C_{31}	102.1 (7)
C_{a3}-C_{b3}-C_{b4}	107.2 (6)	N_5-C_{29}-C_{30}	112.8 (9)
C_{a4}-C_{b4}-C_{b3}	106.6 (6)	N_5-C_{31}-N_6	113.4 (8)
C_{a5}-C_{b5}-C_{b6}	107.0 (6)	C_{29}-C_{30}-N_6	105.9 (9)
C_{a6}-C_{b6}-C_{b5}	107.0 (6)	C_{30}-N_6-C_{31}	105.7 (7)
C_{a7}-C_{b7}-C_{b8}	107.1 (6)	C_{30}-N_6-C_{32}	127.1 (8)
C_{a8}-C_{b8}-C_{b7}	106.8 (6)	C_{31}-N_6-C_{32}	126.7 (8)
C_{a8}-C_{m4}-C_{a1}	124.1 (6)	N_6-C_{32}-C_{33}	111.8 (8)
C_{a2}-C_{m1}-C_{a3}	122.7 (6)	C_{32}-C_{33}-C_{34}	111.1 (9)
C_{a4}-C_{m2}-C_{a5}	124.5 (6)	C_{33}-C_{34}-C_{35}	117.7 (11)
C_{a6}-C_{m3}-C_{a7}	121.9 (6)	C_{34}-C_{35}-C_{36}	117.4 (10)
C_{a1}-C_{m4}-C_{19}	117.3 (6)	C_{35}-C_{36}-N_7	113.9 (8)
C_{a2}-C_{m1}-C_1	118.4 (5)	C_{35}-C_{36}-O	123.5 (11)
C_{a3}-C_{m1}-C_1	118.9 (5)	N_7-C_{36}-O	122.4 (10)
C_{a4}-C_{m2}-C_7	118.1 (5)	C_{36}-N_7-C_{20}	129.3 (7)
N_1-Fe-S	97.0 (2)	N_4-Fe-S	94.4 (2)
N_2-Fe-S	86.6 (2)	N_5-Fe-S	173.8 (2)
N_3-Fe-S	86.8 (2)		

[a] The estimated standard deviations of the least significant digits are given in parentheses.

ligand-orientating effects of the protein almost certainly differ from the essentially unconstrained model. A heme octapeptide–methionine complex is reported[40] to have g values (2.91, 2.31, 1.51) more closely matching our model than cytochrome c, giving further

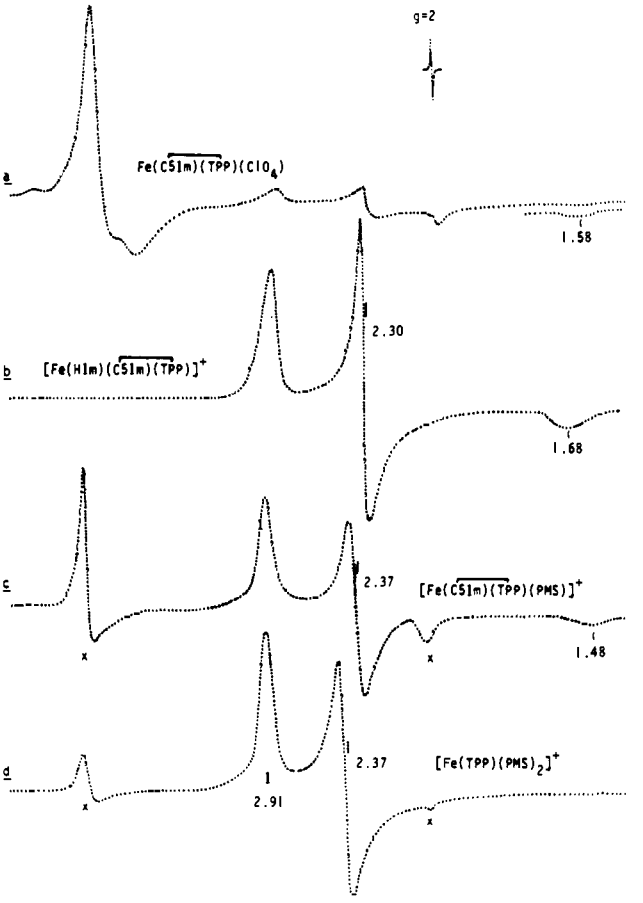

Figure 9. EPR spectra in methylene chloride/chloroform (10 K) for (a) Fe(C5Im)(TPP)(ClO_4) showing both low-spin (g = 2.86, 2.28, 1.58) and high-spin (g = 5.90, 1.99) signals, (b) low-spin bis-N-ligated [Fe(HIm)(C5Im)(TPP)] (g = 2.90, 2.30, 1.68), (c) the EPR spectrum resulting from the addition of pentamethylene sulfide to Fe(C5Im)(TPP)(ClO_4) (g = 2.90, 2.37, 1.48) (bands marked (×) are due to a high-spin species (see text), and (d) [Fe(TPP)$(PMS)_2$]ClO_4 (g = 2.91, 2.37).

evidence that the methionine orientation affects the spin delocalization.[39]

The failure to isolate a crystalline ferricytochrome c analogue, or its precursor, underscores the difficulty of manipulating dissimilar axial ligation in ferric porphyrins. Charge neutralization is a major driving force for the coordination of anions, even so-called weakly coordinating anions like perchlorate. The failure to observe thioether coordination in earlier model studies[15] probably results from unrecognized competition from coordinating anions.

Ideally, the most instructive structural comparison of an Fe(II)/Fe(III) redox pair would be made on the mixed-ligand models having thioether and imidazole coordination. However, lacking a crystalline ferric derivative, we investigated other iron porphyrins having thioether ligation. One other thioether derivative has been reported, but precise data are unavailable from its crystal structure.[41] Accordingly, a redox pair of low-spin bis(thioether) complexes were prepared for structural comparison. The synthetically straightforward iron(II) complex, $Fe(THT)_2(TPP)$ (**5**), was isolated as diamagnetic purple crystals. The successful synthesis of the iron(III) analogue, $[Fe(THT)_2(TPP)]ClO_4 \cdot 1.5CHCl_3$ (**6**), required the use of a chlorinated hydrocarbon as solvent and a large excess of tetrahydrothiophene. The relatively poor structural data obtained for this complex led us to prepare the closely related pentamethylene sulfide complex [Fe(PMS)$_2$-

(40) Abstract of Yang, E. K.; Vickery, L.; Sauer, K. In "Interaction Between Iron and Proteins in Oxygen and Electron Transport", Ho, C., et al., Eds.; Elsevier/North Holland: New York, in press.

(41) Jameson, G. B.; Robinson, W. T.; Collman, J. P.; Sorrell, T. N. *Inorg. Chem.* **1978**, *17*, 858–864.

Table XVIII. Geometry of the Coordination Groups of Selected Hemes and Cytochrome c[a]

heme	dist, Å				angles, deg			
	$Fe-N_p$	$Fe-S_{ax}$	$Fe-N_{ax}$	Δ, core	$Fe-N_{Im}$[c]	$Fe-S_{ax}$[c]	ϕ[d]	ref
$Fe(THT)_2(TPP)$ (5)	1.996 (6)	2.336 (3)		0		4.0		this work
$[Fe(THT)_2(TPP)]ClO_4$ (6)	1.985 (3)	2.357 (27)		0		3.6		this work
$[Fe(PMS)_2(TPP)]ClO_4$ (7)	1.982 (6)	2.341 (17)		0.02		4.4		this work
Fe(C5Im)(TPP)(THT) (1)	1.99 (1)	2.31 (1)	2.00 (1)	0.06[b]	2.4	7.0	3.5	this work
$Fe(1\text{-MeIm})_2TPP$	1.997 (4)		2.014 (5)	0	e		10, 10	47
$[Fe(HIm)_2(TPP)]Cl$	1.989 (4)		1.974 (24)	0.01	~3.5		18, 39	48
$Fe^{III}(1\text{-MeIm})_2(PP\text{-IX})$	1.99 (2)		1.977 (16)	0.03	~1		3, 16	49
ferrocytochrome c	2.06	2.32	1.97	0.06[b]	2.7	5.7	47	18
ferricytochrome c	2.05	2.27	2.00	0.02[b]	5.1	10.1	51	18

[a] The numbers in parentheses are the estimated standard deviation for a single value or, for averaged values, that calculated on the assumption that the values are drawn from the same population. [b] Displacement toward the imidazole ligand. [c] Angle between heme plane normal and axial vector. [d] The angle ϕ is the dihedral angle between the imidazole plane and coordinate planes containing opposite pyrrole nitrogen atoms. [e] Not available.

$(TPP)]ClO_4 \cdot 3CHCl_3$ (7). That thioethers bind sufficiently strongly to form six-coordinate complexes with iron(III) and that their ligand field strengths are sufficiently high to yield low-spin complexes ($\mu = 2.1\ \mu_B$) are notable. Thioethers have frequently been considered very poor ligands, particularly toward metals in higher oxidation states.[42] There is clearly no need to invoke any special protein enforcement of methionine binding in ferricytochrome c. The thioether ligand affinities are, however, considerably weaker than imidazole and several properties illustrate this. Crystalline samples of **6** and **7** aged with a persistent garlic odor from a gradual egress of the thioether. This aging was accompanied by an increase in the magnetic moment. Attempted alternative syntheses with different solvents and thioethers frequently failed, producing $Fe(OClO_3)(TPP)$ instead. EPR spectra of **6** and **7** in frozen 2-methyltetrahydrofuran solution showed signals almost entirely due to $Fe(OClO_3)(TPP)$. In $CHCl_3/CH_2Cl_2$, however, the low-spin signals of **6** and **7** ($g = 2.91, 2.37$) were predominant (see Figure 9d). There has been one report of an equilibrium constant in an iron(II) cytochrome c model, 8 M^{-1}, for methyl propyl sulfide.[16]

In ferricytochrome c, a weak absorption band at 695 nm is a widely accepted criterion of methionine ligation.[3] Some of our iron(III) thioether ligated complexes show weak bands above 650 nm but then so do certain non-thioether-containing iron(III) tetraphenylporphyrin complexes such as Fe(Cl)(TPP). The usual lack of congruence between UV and visible spectra of naturally occurring hemes and TPP derivatives (which frequently have more bands) does not allow firm assignments to be made at this time.

The synthesis of **1** has allowed electrochemical investigations to determine the effect on the redox potential of substituting a thioether for an imidazole in bis-ligated low-spin iron porphyrins. A complete description of these studies has been reported elsewhere.[43] The redox potential of **1** (vs. SCE; THF solution) is 185 ± 10 mV, and the redox potential for the complex in which THT is replaced by 1-MeIm is 18 ± 10 mV. Thus, there is a 167-mV positive shift in E arising from the imidazole → thioether ligation change. This is in reasonable agreement with the ~150-mV shift observed for a parallel ligand substitution in Harbury's aqueous heme octapeptide system[11] and also in Wilson's dioxane/water study with mesoheme derivatives (+~146 mV).[44] Collectively, these results yield a thioether ligand effect of ~160 mV more positive than imidazole. The agreement from three independent studies in three quite different media suggests that this axial ligand effect can be considered intrinsic and can be safely partitioned from any environment effects. When the same axial ligand change (histidine to methionine) is observed in cytochromes, differences of ~460 mV between c_3 and c and ~90 mV between b_5 and b_{562} are found. This illustrates the profound effects that the protein environment has on the redox potential in the cytochromes. This effect may be additive with the thioether ligation effect as with c_3 and c or it may be in opposition as with b_5 and b_{562}. The origin of these environment effects is uncertain,[43,45,46] but must be related to stabilization or destabilization of the positive charge on the oxidized heme.

Structural Aspects. The averaged bond distances of the coordination groups of the four thioether derivatives reported herein are collected in Table XVIII along with the comparable data for three bis(imidazole) complexes reported previously.[47-49] The $Fe-N_p$ lengths show the small expected decreases between the ferrous and ferric oxidation states. The ferric derivative, **7**, and the ferrous tailed derivative, **1**, show $Fe-N_p$ distances that are slightly shorter than the average distance observed for all low-spin ferric and ferrous derivatives, respectively.[27] This is the consequence of modest ruffling in the cores of these derivatives, presumably due to crystal-packing influences.

A chemically significant feature of these structures is the axial Fe–S bond lengths. The two independent half-molecules of the *ferrous* derivative, **5**, have Fe(II)–S distances that are almost identical at 2.334 (1) and 2.338 (1) Å. The average Fe(III)–S distance of the *ferric* complex, **7**, is essentially the same; the two individual values are found to be slightly shorter, 2.329 (2) Å, and slightly longer, 2.353 (2) Å, than the Fe(II)–S distance. A similar pattern is observed for the less precisely determined structure of **6** where the two Fe(III)–S are 2.338 (2) and 2.376 (4) Å. This small asymmetry in the axial Fe(III)–S bonds may be the result of packing forces; it is interesting to note that the same type of asymmetry is observed in the axial Fe(III)–N bonds of the bis(imidazole) derivatives listed in Table XVIII. These results suggest that the Fe–S(thioether) bond lengths are essentially independent of oxidation state, unlike the bis(imidazole) case where there is a small but real difference of ~0.04 Å between the ferrous and ferric porphyrins. The expected increase in Fe–S upon oxidation due to poor compatibility of the "hard" Fe(III) for the "soft" thioether ligand[50] is apparently offset by the increased charge attraction of Fe(III) for its ligands. The independence of the Fe–S(thioether) bond lengths to the oxidation state of the iron porphyrin is paralleled by the very narrow range of observed Fe–S bond lengths in all presently known (porphinato)iron derivatives despite changes in the nature of the sulfur ligand, the oxidation state of the iron, and the spin state and the

(42) Amundsen, A. R.; Whelan, J.; Bosnich, B. *Inorg. Chem.* **1979**, *18*, 206-208.
(43) Marchon, J.-C.; Mashiko, T.; Reed, C. A. In "Interaction Between Iron and Proteins in Oxygen and Electron Transport", Ho, C., et al., Eds.; Elsevier/North Holland: New York, in press.
(44) Wilson, G. S. *Bioelectrochem. Bioenerg.* **1974**, *1*, 172-179.
(45) Kassner, R. J. *Proc. Natl. Acad. Sci. U.S.A.* **1972**, *69*, 2263-2267.
(46) Stellwagen, E. *Nature (London)* **1978**, *275*, 73-74.
(47) Steffen, W. L.; Chen, H. K.; Hoard, J. L.; Reed, C. A. "Abstracts of Papers", 175th National Meeting of the American Chemical Society, Anaheim, CA, March 1978; American Chemical Society: Washington, D.C., 1978; INOR 15.
(48) Collins, D. M.; Countryman, R.; Hoard, J. L. *J. Am. Chem. Soc.* **1972**, *94*, 2066-2072.
(49) Little, R. G.; Dymock, K. R.; Ibers, J. A. *J. Am. Chem. Soc.* **1975**, *97*, 4532-4539.
(50) Pearson, R. G. *J. Chem. Educ.* **1968**, *45*, 581-587, 643-648.

coordination number of the complex. Thus the Fe–S bond lengths in the high-spin thiolato iron(III) (2.324 (2) Å)[51] and iron(II) (2.360 (2) Å)[52] derivatives are quite close to the low-spin Fe–S(thioether) distances reported here. Moreover, for the iron(II)–thiolato derivative, the Fe–S distance changes very little (to 2.352 (2) Å)[52] upon coordination of CO which converts the molecule to a low-spin state.[53-55] While there are too few data on Fe–S bond lengths in model complexes to be certain, these data suggest that unconstrained hemoproteins (cytochrome *c*, P-450, etc.) will have Fe–S distances falling close to this range. Refined X-ray structures of reduced and oxidized cytochrome *c* put the Fe(II)–S distance at 2.32 Å and the Fe(III)–S distance at 2.27 Å.[18] A complete comparison of the coordination groups of the thioether-containing hemes and ferro- and ferricytochrome *c* is given in Table XVIII.

The model compound studies reported herein thus suggest that minimal changes will occur in the heme coordination group of cytochrome *c* upon valency change. Recent EXAFS studies of Labhardt and Yuen[56] and Moffat and Korszun[57] are in agreement on this point; the EXAFS studies indicate bond length changes of <0.01 Å upon redox. Interestingly, the Moffat and Korszun studies included a number of cytochrome *c* derivatives with a wide range of midpoint potentials. The refined crystallographic results for tuna cytochrome *c*[18] are also consonant with minimal coordination group changes on redox. All of these results appear to disagree with the suggestion of Moore and Williams[58] that variation in redox potential for cytochrome *c* is correlated with changes in Fe–S lengths.

A significant question concerning the use of covalently attached ligands or similar strategies to prepare synthetic analogues is the possible effects that these may have on the structure of the analogue. The use of an imidazole tail in Fe(C5Im)(TPP)(THT) appears to have had an insignificant effect on its structure. The conformation of the porphinato core and the orientation of the phenyl ring bearing the tail substituent are well within the range of normal values. Consideration of the observed structure and scaled molecular models suggests that a C4Im tail or possibly even a C3Im tail would allow complex formation although the range of orientations of the imidazole plane with respect to the Fe–N(porphyrin) coordination planes would be limited. The observed orientation of the imidazole ring with a ϕ angle of 4° with the N5FeN2 coordinate plane engenders moderately close nonbonded distances between imidazole hydrogen atoms and atoms of the core (~2.55 Å). Examination of models suggests that the observed orientation is not a consequence of the attached tail. Similar alignments of coordinated imidazole along a M–N(porphyrin) bond have been observed in a number of metalloporphyrin derivatives.[59-61] The frequency of this alignment suggests electronic considerations may be an important factor. In hemoproteins, however, the imidazole plane orientation is typically at $\phi \simeq 45°$ rather than $\simeq 0°$; this is the case for both oxidized and reduced cytochrome *c*.[18] This systematic difference in the orientation of the imidazole ligand of model complexes compared to the hemoproteins suggests that the orientation of the imidazole may be controlled by the protein. In this cytochrome *c* model, the Fe(II)–N(imidazole) bond distance of 2.00 (1) Å is essentially the same as that of Fe(1-MeIm)$_2$(TPP)[47] and the Fe(II)–S distance is the same as that found for the bis(thioether) derivatives (Table XVIII). Thus, within the precision of the structure determination, there does not appear to be any synergic bonding effects caused by the dissimilar axial ligands.

The 3–7° off-axis tilting of the Fe–S vector observed in all the thioether derivatives may result from minimizing nonbonded contacts between the α-hydrogen atoms of the sulfur ligands and porphinato core atoms. Calculated H···core atom separations range upward from 2.55 Å, and the ligand orientations are such that decreasing the off-axis tilt of Fe–S would decrease the H···core atom separations. A similar off-axis tilt of the Fe–S(met 80) vector is seen in tuna cytochrome *c*.[18]

The C–S–C angles in [Fe(PMS)$_2$(TPP)]ClO$_4$ (average 99.4 (7)°) are comparable to those observed in complexes with alkyl sulfides;[62] the corresponding angles in the THT complexes are significantly smaller at 92.9 (5)°. It is unlikely that there are significant differences in the coordination properties of open-chain alkyl sulfides compared to the cyclic thioethers, in distinct contrast to ethers where the cyclic ether THF is a significantly better ligand than the open-chain ethers. The steric factors leading to a more accessible oxygen atom in cyclic ethers, compared to open-chain ethers, are much less significant in the thioethers as a result of the ~0.4 Å longer C–S bonds. Moreover, the basicities of alkyl and cyclic thioethers lie in a narrower range than those of the ethers.[63] We thus believe that the cyclic thioethers used in this study are adequate structural models for coordination of methionine to iron porphyrins.

Conclusions. The model compound studies presented herein suggest that minimal change is expected in the Fe–S bond lengths in cytochrome *c* upon valency change because this is an intrinsic property of thioether ligation. As a rule, coordination bond length changes of less than 0.05 Å do not contribute significant Franck–Condon barriers to electron transfer[5] so that in cytochrome *c*, Franck–Condon effects are not expected to have a major influence on the rate of electron transfer. The successful synthesis of the iron(III) bis(thioether) derivatives makes evident that no special protein constraints are needed to achieve methionine coordination in low-spin cytochromes *c*, other than to minimize access to the coordination site by higher affinity ligands. The electrochemical results for **1** provide a good estimate of the +160-mV intrinsic effect on the redox potential of replacing a histidine ligand with a methionine ligand in a low-spin cytochrome. These studies have also demonstrated the utility of the tail porphyrin concept in providing metalloporphyrin complexes with prescribed pairs of axial ligands.

Acknowledgment. We thank Dr. T. Takano for very kindly providing preprints of ref 18. We thank Professor K. Moffat and Dr. R. Korszun for discussion of their EXAFS results. We acknowledge support of this work by the National Institutes of Health through Grants GM-25851 (C.A.R.) and HL-15627 (W.R.S.).

Supplementary Material Available: Tables of atomic coordinates and temperature factors for all four crystal structures and bond distances and angles for [Fe(THT)$_2$(TPP)]ClO$_4$ (Tables II–XI) and listings of observed and calculated structure amplitudes (×10) for all four crystal structures (156 pages). Ordering information is given on any current masthead page.

(51) Tang, S. C.; Koch, S.; Papaefthymiou, G. C.; Foner, S.; Frankel, R. B.; Ibers, J. A.; Holm, R. H. *J. Am. Chem. Soc.* **1976**, *98*, 2414–2434.
(52) Caron, C.; Mitschler, A.; Riviera, G.; Ricard, L.; Schappacher, M.; Weiss, R. *J. Am. Chem. Soc.* **1979**, *101*, 7401–7402.
(53) A possible exception to these observations is a thiol, thiolate complex, Fe(TPP)(C_6H_5S)(C_6H_5SH). The magnetic[54] and structural[55] behavior this material is quite complex; an apparent six-coordinate form of the molecule has Fe–S = 2.27 and 2.43 Å.
(54) McCann, S. W.; Wells, F. V.; Wickman, H. H.; Sorrell, T. N.; Collman, J. P. *Inorg. Chem.* **1980**, *19*, 621–628.
(55) Collman, J. P.; Sorrell, T. N.; Hodgson, K. O.; Kulshrestha, A. K.; Strouse, C. E. *J. Am. Chem. Soc.* **1977**, *99*, 5180–5181. Strouse, C. E., personal communication.
(56) Labhardt, A.; Yuen, C. *Nature (London)* **1977**, *277*, 150–151.
(57) Moffat, K.; Korszun, R., personal communication.
(58) Moore, G. R.; Williams, R. J. P. *FEBS Lett.* **1977**, *79*, 229–232.
(59) Scheidt, W. R. *J. Am. Chem. Soc.* **1974**, *96*, 90–94.
(60) Little, R. G.; Ibers, J. A. *J. Am. Chem. Soc.* **1974**, *96*, 4452–4463.
(61) Kirner, J. F.; Reed, C. A.; Scheidt, W. R. *J. Am. Chem. Soc.* **1977**, *99*, 2557–2563.
(62) Elder, R. C.; Kennard, G. J.; Payne, M. D.; Deutsch, E. *Inorg. Chem.* **1978**, *17*, 1296–1303.
(63) Huheey, J. E. "Inorganic Chemistry", 2nd ed.; Harper and Row: New York, 1978; pp 271–276.